SEMMELWEIS EGYETEM

DOKTORI ISKOLA

Ph.D. értekezések

3305.

SASVÁRI PÉTER

Celluláris és molekuláris élettan

című program

Programvezető: Dr. Hunyady László, egyetemi tanár

Témavezető: Dr. Csépányi-Kömi Roland, egyetemi docens

Interactions and Phosphorylation-Dependent Roles of ARHGAP25 in Neutrophils

PhD thesis

Péter Sasvári

Semmelweis University Doctoral School

Molecular Medicine Division

Supervisor:	Dr. Roland Csépányi-Kömi, PhD
Official reviewers:	Dr. Bőgel Gábor, PhD
	Dr. Pap Ádám, PhD
Head of the Complex Examination Committee:	Dr. Nándor Nagy, PhD DSc
Members of the Complex Examination Committee:	Dr. Noémi Sándor, PhD
	Dr. Zoltán Pós, PhD

Budapest

2025

Table of Contents

List of Abbreviations

Akt	–	Protein kinase B
ANN	–	Artificial Neural Network (scoring)
ANOVA	–	Analysis of Variance
AP-MS	–	Affinity Purification-coupled Mass Spectrometry
ARMS	–	Alveolar Rhabdomyosarcoma
ASCL2	–	Achaete-Scute Family BHLH Transcription Factor 2
ATP	–	Adenosine Triphosphate
BioID	–	Proximity-Dependent Biotin Identification (method)
BRET	–	Bioluminescence Resonance Energy Transfer
CC	–	Coiled-Coil (domain)
CFP	–	Cyan Fluorescent Protein
ChIP	–	Chromatin Immunoprecipitation
DNA	–	Deoxyribonucleic Acid
DTT	–	Dithiothreitol
EDTA	–	Ethylenediaminetetraacetic Acid
ERMS	–	Embryonal Rhabdomyosarcoma
FBS	–	Fetal Bovine Serum
FC	–	Fold Change
FRET	–	Förster Resonance Energy Transfer
GAP	–	GTPase-Activating Protein
GDI	–	Guanine Nucleotide Dissociation Inhibitor
GDP	–	Guanosine Diphosphate
GDPβS	–	Guanosine 5′-(β-thio-)diphosphate
GEF	–	Guanine Nucleotide Exchange Factor
GO	–	Gene Ontology
GPCR	–	G Protein-Coupled Receptor
GST	–	Glutathione S-Transferase

GTP	–	Guanosine Triphosphate
GTPγS	–	Guanosine 5′-(γ-thio-)triphosphate
HCD	–	Higher-energy Collisional Dissociation
HEK	–	Human Embryonic Kidney (cells)
HIF1α	–	Hypoxia-Inducible Factor 1-alpha
HRAS	–	Harvey Rat Sarcoma Viral Oncogene Homolog
HSPC	–	Hematopoietic stem and progenitor cell
IgG	–	Immunoglobulin G
ipTM	–	Interfacial Predicted Template Modeling (AlphaFold metric)
KO	–	Knock-out
LC-MS/MS	–	Liquid Chromatography-coupled Tandem Mass Spectrometry
LDHA	–	Lactate Dehydrogenase A
LFQ	–	Label-Free Quantification
MFI	–	Mean Fluorescence Intensity
MMP	–	Matrix Metalloproteinase
MTOR	–	mammalian target of rapamycin
NADPH	–	Nicotinamide Adenine Dinucleotide Phosphate (Reduced)
NK	–	Natural Killer (cells)
NOX2	–	NADPH Oxidase 2
ORF	–	open reading frame
PAE	–	Predicted Aligned Error (AlphaFold metric)
PAK1	–	p21-Activated Kinase 1
PAK-PBD	–	PAK1 p21-Binding Domain
PBS	–	Phosphate-buffered saline
PBST	–	PBS containing 0.1% Tween-20
PCA	–	Principal Component Analysis
PCNA	–	Proliferating Cell Nuclear Antigen
PCR	–	Polymerase Chain Reaction

PH	–	Pleckstrin Homology (domain)
PI3K	–	Phosphoinositide 3-Kinase
PKM2	–	Pyruvate Kinase M2
PLA	–	Proximity Ligation Assay
PMSF	–	Phenylmethylsulfonyl Fluoride
PPI	–	Protein–Protein Interaction
RNA	–	Ribonucleic Acid
ROCK	–	Rho-associated Protein Kinase
RPMI	–	Roswell Park Memorial Institute (medium)
SNAI1	–	Snail Family Transcriptional Repressor 1
STRING	–	Search Tool for the Retrieval of Interacting Genes/Proteins
SUMO	–	Small Ubiquitin-like Modifier
SVM	–	Support Vector Machine (scoring)
TM	–	Triple mutant
WT	–	Wild Type
Y2H	–	Yeast Two-Hybrid
YFP	–	Yellow Fluorescent Protein

1. Introduction

1.1. Small G proteins

1.1.1. Brief history of G protein research

The discovery of *G proteins* marks one of the major advancements in biology that was awarded a Nobel Prize in Physiology or Medicine in 1994 (1). Alfred G. Gilman and Martin Rodbell, the two laureates—alongside their coworkers—began searching for answers to a phenomenon that had been troubling the scientific community in the 1970s: how signal conversion takes place at the cell membrane. Their extensive work led to the discovery that heterotrimeric G proteins play an essential role in the functioning of *G protein-coupled receptors* (GPCRs), which would later be identified as vital in numerous physiological processes, including sensory perception, immune responses, and neurotransmission (2). The relevance of these proteins is further demonstrated by the fact that three additional Nobel Prizes, awarded in 2000, 2004, and 2012, are also connected to GPCRs (1).

Unexpectedly, another family of proteins was later identified (3) with similar guanosine triphosphate (GTP) hydrolyzing properties. However, these were composed of a single polypeptide chain, hence receiving the name *monomeric or 'small' GTPases*. Even though the α subunit of heterotrimeric GTPases shows a similar biochemical behavior, small G proteins orchestrate a plethora of different yet indispensable intracellular processes (4), rendering them a hot topic in numerous fields of molecular physiology.

1.1.2. Small G protein structure and regulation

One of the most significant breakthroughs in understanding small GTPases was identifying their three-dimensional structures. HRAS was the first to have the crystal structure of its G-domain elucidated (5), providing a foundation for understanding the structural attributes of many other Ras-family members. All members share a secondary structure of five highly conserved '*G motifs*' that provide contact surface and interaction sites for the nucleotide and the magnesium ion (4). The N- and C-terminal extensions around the GTPase domain vary greatly among the family members, which is responsible for their differences in subcellular localization and binding specificity for interactions (Figure 1A).

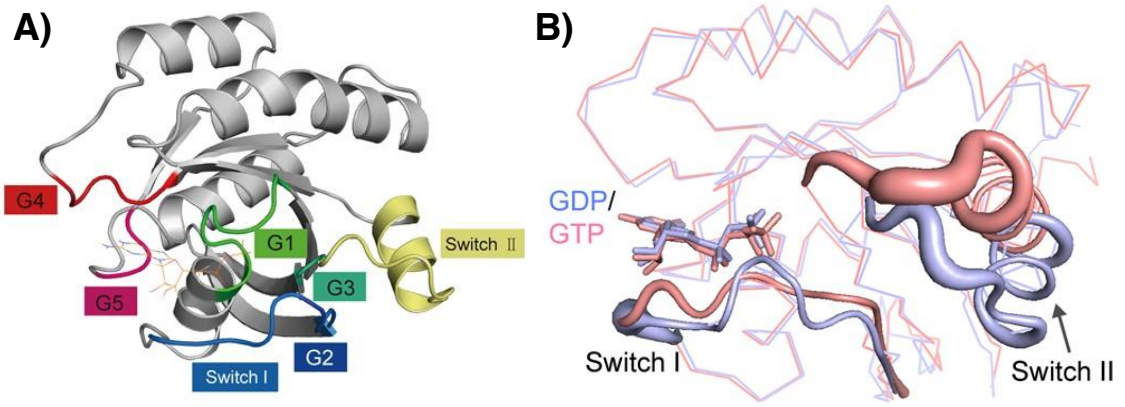

Figure 1. The general structure of monomeric GTPases. *A) Schematic model of a small GTPase with the G motifs (G1-5) and the GTP-binding pocket. B) Conformational changes in the switch regions between the GDP- (light purple) and the GTP-bound state (pink). The drawings are taken from Figure 1 of Yin et al.(4).*

The binding of GTP to the protein is indispensable for its activation. This event is facilitated by the GTP-GDP ratio shifted in favor of GTP in healthy, living cells (6), hence significantly increasing its probability. Since only the GTP-bound GTPase is capable of taking part in cellular processes (7), it is referred to as the active form. The GDP- and GTP-bound protein structures of small GTPases have conformational differences (4) localized in two regions (switch I and switch II). Compared to the more flexible structure in the GDP-bound state, they adopt a more ordered conformation upon GTP-binding due to the presence of the γ phosphate that creates new and alters existing secondary bonds with and within the protein (Figure 1B).

Most GTPases can hydrolyze GTP, and the cleaving of the phosphate group renders the GTPase itself inactive (7). Nevertheless, the intrinsic enzymatic activity of the GTPases is kinetically inadequate to keep up with the pace of the ever-changing intracellular milieu of the cell. This kinetic hindrance is alleviated by *GTPase-activating proteins* (GAPs), by assisting in their deactivation (8), which ensures the silencing of the GTPase-driven signaling pathways. This also opens the possibility for a new cycle, as the GDP-bound form can be reactivated by exchanging the bound GDP for GTP. However, this process requires additional proteins, called *guanine nucleotide exchange factors* (GEFs**)**, responsible for the detachment of GDP (9).

In a small subset of GTPases, another family of proteins was confirmed to add to this relatively simple cycle. The *guanosine dissociation inhibitors* (GDIs) can sequester the inactive GTPases (10) and keep them away from the cell membrane by masking the lipid-binding part of the G proteins. Their relocation from the intracellular membranes to the cytoplasm serves a dual purpose: apart from its evident inhibitory effect, the soluble complex also doubles as protection against protein degradation (10). The described GTP/GDP cycle is summarized in Figure 2.

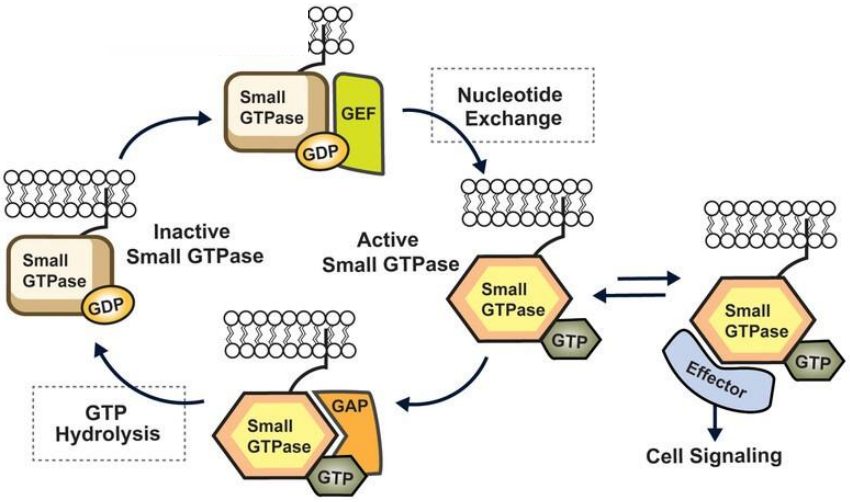

Figure 2. Activation cycle of small GTPases*. Monomeric GTPases are typically anchored to the plasma membrane. The GDP-bound (inactive) form can be converted into the GTP-bound (active) form by GEFs. The active form can bind to various effector molecules and induce intracellular processes. GAPs catalyze the intrinsic hydrolytic activity of small GTPases, which renders the protein inactive. The GTP-bound small GTPase takes part in cell signaling via different effector proteins. The drawing is taken from Figure 1 of Faulkner et al. (11).*

1.1.3. The Ras superfamily

Monomeric G proteins comprise a single polypeptide chain of 20–30 kDa (11). Even though their structure and biochemical properties are evolutionarily conserved, they execute a wide range of tasks inside the cells, such as cell proliferation, differentiation, adhesion, migration, survival, and apoptosis (12). This aligns with the observation (13) that the absence or malfunction of these proteins is responsible for several diseases. The Ras proteins were one of the first small GTPases to be discovered (5). Initially identified

as oncogenes with the potential to cause cancer when mutated (12), they were the first puzzle piece to link small GTPases to the aforementioned cellular processes, generating a hotspot for biochemical research to understand their additional functions in the cell.

Now, the number of current Ras superfamily members exceeds 150 (14), grouped into five classes based on structure and function (Ras, Rho, Rab, Ran, and Arf). Due to the magnitude of the topic, only the Rho family is discussed in detail in the next section.

1.1.4. Rho family GTPases in detail

The word 'Rho' is a portmanteau coined by the merging of '*Ras homogenous*', referring to the fact that Rho family members closely resemble Ras (15). Generally, at least one of the 20 members is present in any cell, as they play a key role in essential processes, such as the organization of the cytoskeleton, cell adhesion, polarity, motility, cell cycle progression, and even gene expression (16). Consequently, they orchestrate processes relevant to inflammation, tumor progression, and wound healing, among others (16-19). Besides the conserved G domain, most members possess a C-terminal hypervariable region ending with a *CAAX* sequence (C stands for cysteine, while A and X could be an aliphatic or any amino acid, respectively) (20). This motif plays a key role in subcellular localization after being modified by, *e.g.,* isoprenylation or carboxyl methylation (20).

Currently, we distinguish eight subclasses (21) based on functional and structural homology (as depicted in Figure 3), but the members can also be divided into classical and atypical GTPases. While classical Rho-family GTPases function as previously described, atypical GTPases are locked in their GTP-bound active form, and there is no current evidence of their regulation by GEFs or GAPs (17).

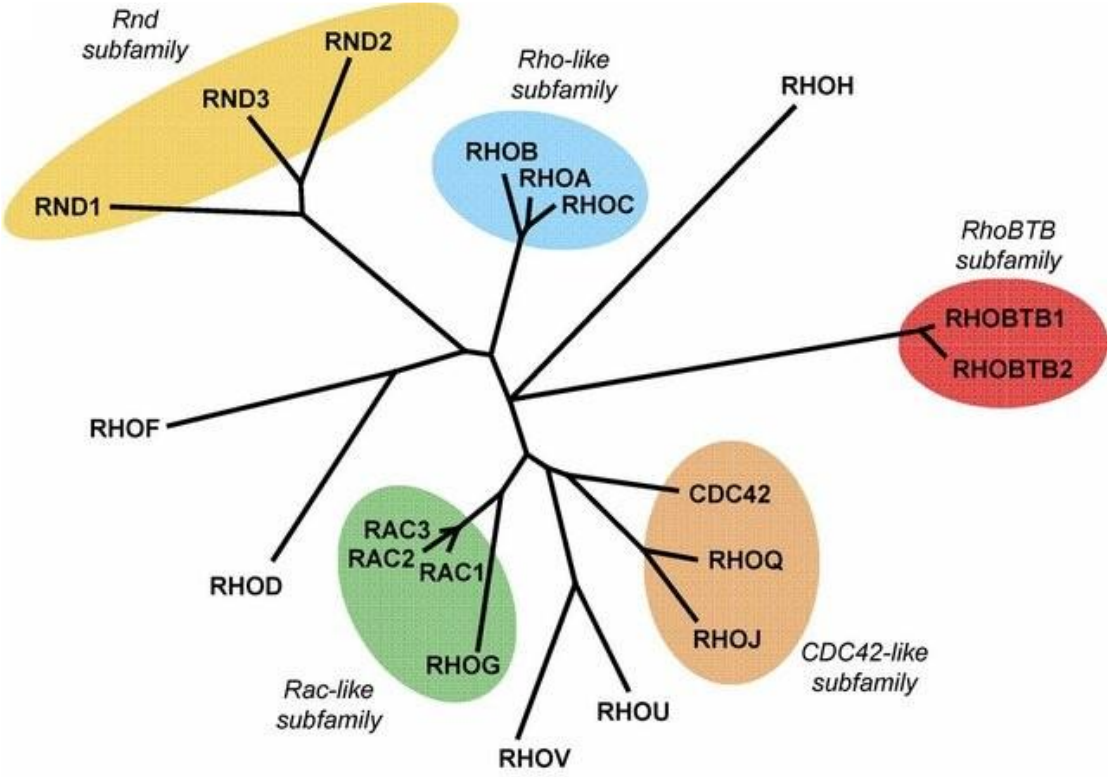

Figure 3. Phylogenetic tree of the Rho family. *Currently, twenty proteins are considered to be members of the Rho family. Due to the close similarity among certain members, they can be further divided into subfamilies. Members of the Rho, Rac, Cdc42, and RhoF subfamilies are considered as classical Rho-family proteins. In contrast, members of the Rnd and RhoBTB subfamilies [RHOBTB3 not shown], RHOU, RHOV, and RHOH, are called atypical due to their altered intracellular behavior. The drawing is taken from Figure 2 of Lawson et al. (21).*

1.1.4.1. Classical Rho-family proteins

The classical Rho family is comprised of 4 subclasses: *Rho* (members: RHOA, RHOB, RHOC), *Rac* (members: RAC1, RAC2, RAC3, RHOG), *Cdc42* (members: CDC42, RHOQ, RHOJ), and *RhoF* (members: RHOF, RHOD). All classical members are regulated by GDP/GTP exchange, which is coordinated by the harmonious work of approximately 80 RhoGEFs, 70 RhoGAPs, and three GDIs (22). Depending on the surrounding protein milieu, multiple regulators and effector proteins can be associated with the active Rho-family GTPases (23), rendering them a versatile asset in cellular

processes. The overlap in regulators and effectors varies among members, and its relevance in cell biology is still laden with unanswered questions. Most of our current knowledge is obtained from studies about the three 'oldest' members: RHOA, RAC1, and CDC42. They are key players in remodeling the actin cytoskeleton, making them essential for cell morphology, polarity, and migration, along with processes not directly linked to actin reorganization (e.g., NADPH oxidase activation, gene expression, apoptosis, and tumorigenesis (16, 18).

1.1.4.2. Atypical Rho-family proteins

Out of the human members, 8 Rho family GTPases have atypical properties, an uncommon feature in the Ras superfamily (24). These proteins are known or predicted to be predominantly GTP-bound in cells due to impaired GDP-GTP exchange or GTP hydrolysis. The proteins have been implicated in diverse functions , including cell adhesion and migration, vesicle trafficking, and cell proliferation (25).

RHOU and RHOV are found to be GTP-loaded in the cell due to their fast GTP cycling ability (26). Rnd subclass members (RND1, RND2, and RND3) and RHOH are special Rho members, as they do not share the amino acids essential for GTP hydrolysis, making them constitutively active (27). RHOBTB1, RHOBTB2, and RHOBTB3 have a characteristic feature of a long C-terminal extension (28). Interestingly, their known intracellular role is not related to cytoskeletal rearrangements but to cullin 3-based ubiquitin ligase complexes (29). Moreover, they are not regulated by GEFs or GAPs but through interaction with other proteins (30, 31).

1.2. ARHGAP25

1.2.1. Protein structure and expression profile

ARHGAP25 is a protein of approximately 73.5 kDa molecular weight, capable of GTPase activation (32). The corresponding gene (formerly known as KIAA0053) is located on chromosome 2p13, which is translated to a protein showing 50% homology with FilGAP (also known as p73RhoGAP and ARHGAP24) (32). It comprises an N-terminal pleckstrin homology (PH) domain closely linked to a RhoGAP domain. The C-terminal end contains a coiled-coil region connected to the RhoGAP domain by a long, disordered sequence (Figure 4). The protein ('Isoform 4') was first isolated from human neutrophils after its *in-silico* identification, and the recombinant protein was

demonstrated to reduce GTP-bound RAC levels *in vitro*, while RHOA and CDC42 were unaffected (33). So far, two mutants, R193A and G218R (numbered according to the amino acid sequence of 'Isoform 4'), have been discovered with impaired GAP activity. The arginine at the 193rd position is a highly conserved, critical catalytic residue in the RhoGAP domain, whose mutation to alanine abolishes the domain's enzymatic ability (33). Even though no cases have been reported with this mutation, exome sequencing identified a novel heterozygous missense variant in a three-generation Finnish family suffering from severe, early-onset, autosomal-dominant skeletal fragility (34). The G218R mutant exhibited impaired RacGAP activity and promoted cell spreading (similar to the R193A mutant) (34).

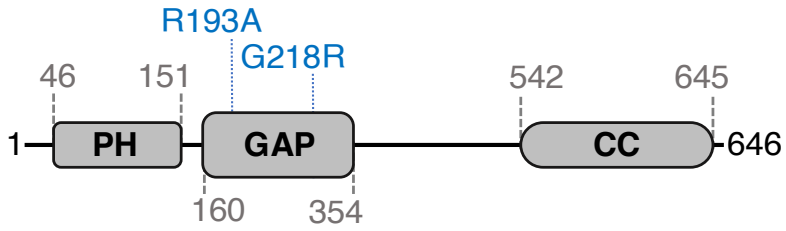

Figure 4. The structure of ARHGAP25 ('Isoform 4'). *The protein contains an N-terminal pleckstrin homology ('PH') domain closely linked to a RhoGAP domain ('GAP'). The coiled-coil sequence ('CC') is located by the C-terminal and linked to the RhoGAP domain by a disordered region. The domains' starting and ending amino acid positions are labelled in gray. The two known mutations causing GAP enzyme deficiency in ARHGAP25 are colored blue. The figure was created by the author.*

Initially, ARHGAP25 was considered a leukocyte-specific protein due to its enrichment in peripheral blood mononuclear cells, spleen, and thymus. Still, since the beginning, measurable amounts of ARHGAP25 mRNA were detected in the heart, the skeletal muscles, the intestines, the kidneys, the liver, the placenta, and the lungs via Northern blot (33). The currently known RNA profile of ARHGAP25—provided as part of the Human Protein Atlas Project (version:24.0; gene: ARHGAP25; accession date: 19.06.2025)—depicts a protein with a tissue- and cell-specific expression pattern (35, 36). Single-cell transcriptomic approaches identified numerous immune cell populations (T

cells, B cells, NK cells, granulocytes, Hofbauer cells, and Kupffer cells) and microglial cells with high mRNA content (Figure 5A). Additionally, excitatory neurons, specific endothelial cells, adipocytes, plasma cells, monocytes, macrophages, dendritic cells, Langerhans cells, and erythroid cells also express ARHGAP25 to a certain degree.

Tissue-wise, the bone marrow and the lymphoid tissues (*e.g.,* spleen, thymus, appendix, lymph nodes, and tonsils) exhibit high expression levels. Still, others, such as the epididymis, ovary, small intestine, and lungs, are moderately enriched in ARHGAP25, aligning with the previously mentioned Northern blot results (Figure 5B).

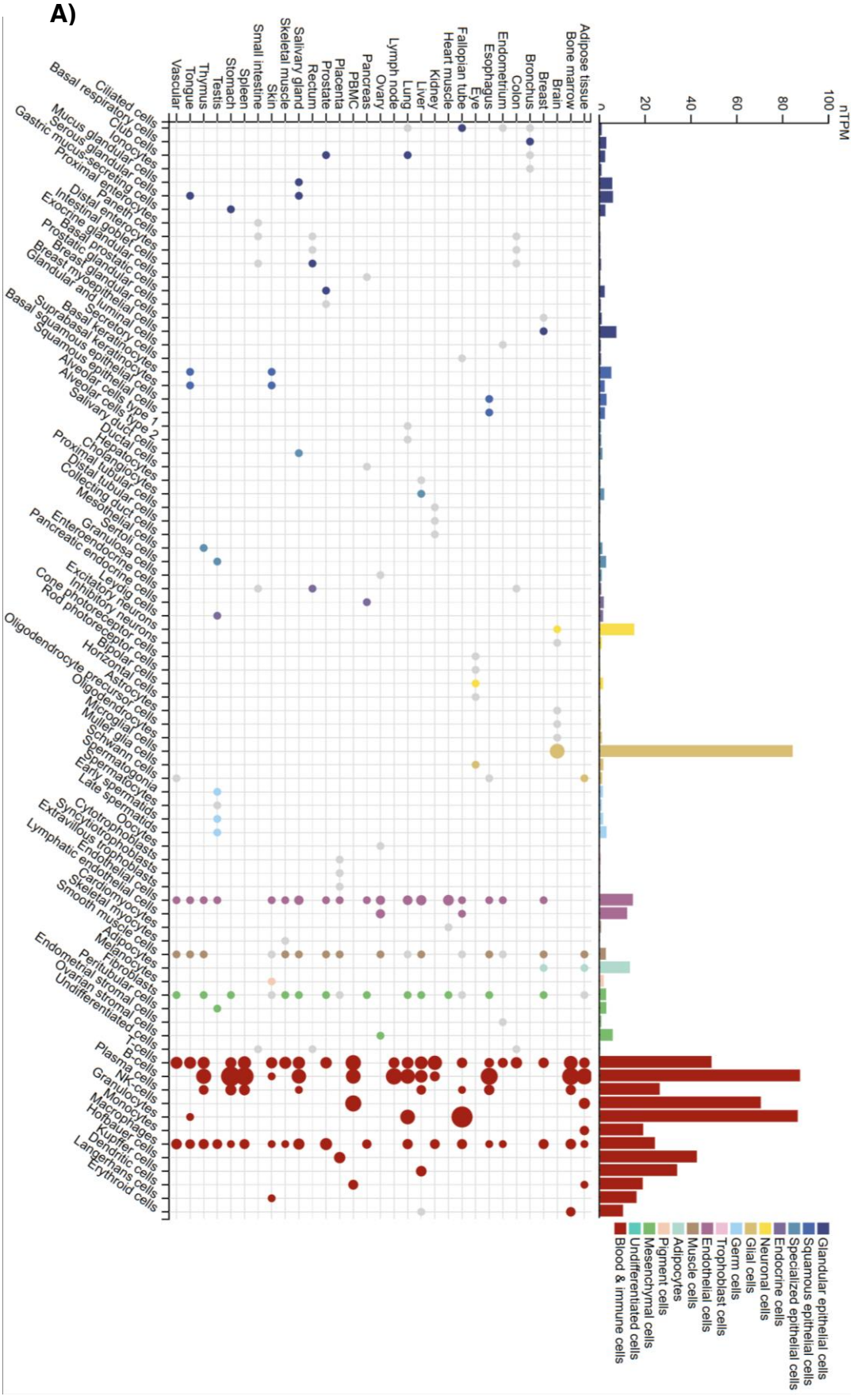
A)
nTPM
0
20
40
60
80
100
Adipose tissue
Bone marrow
Brain
Breast
Bronchus
Colon
Endometrium
Esophagus
Eye
Fallopian tube
Heart muscle
Kidney
Liver
Lung
Lymph node
Ovary
Pancreas
PBMC
Placenta
Prostate
Rectum
Salivary gland
Skeletal muscle
Skin
Small intestine
Spleen
Stomach
Testis
Thymus
Tongue
Vascular
Ciliated cells
Basal respiratory cells
Club cells
Ionocytes
Mucus glandular cells
Serous glandular cells
Gastric mucus-secreting cells
Proximal enterocytes
Distal enterocytes
Paneth cells
Intestinal goblet cells
Exocrine glandular cells
Basal prostatic cells
Prostatic glandular cells
Breast glandular cells
Breast myoepithelial cells
Glandular and luminal cells
Secretory cells
Basal keratinocytes
Suprabasal keratinocytes
Basal squamous epithelial cells
Squamous epithelial cells
Alveolar cells type 1
Alveolar cells type 2
Salivary duct cells
Ductal cells
Hepatocytes
Cholangiocytes
Proximal tubular cells
Distal tubular cells
Collecting duct cells
Mesothelial cells
Sertoli cells
Granulosa cells
Enteroendocrine cells
Pancreatic endocrine cells
Leydig cells
Excitatory neurons
Inhibitory neurons
Cone photoreceptor cells
Rod photoreceptor cells
Bipolar cells
Horizontal cells
Astrocytes
Oligodendrocyte precursor cells
Oligodendrocytes
Microglial cells
Müller glia cells
Schwann cells
Spermatogonia
Spermatocytes
Early spermatids
Late spermatids
Oocytes
Cytotrophoblasts
Syncytiotrophoblasts
Extravillous trophoblasts
Endothelial cells
Lymphatic endothelial cells
Cardiomyocytes
Skeletal myocytes
Smooth muscle cells
Adipocytes
Melanocytes
Fibroblasts
Peritubular cells
Endometrial stromal cells
Ovarian stromal cells
Undifferentiated cells
T-cells
B-cells
Plasma cells
NK-cells
Granulocytes
Monocytes
Macrophages
Hofbauer cells
Kupffer cells
Dendritic cells
Langerhans cells
Erythroid cells
Glandular epithelial cells
Squamous epithelial cells
Specialized epithelial cells
Endocrine cells
Neuronal cells
Glial cells
Germ cells
Trophoblast cells
Endothelial cells
Muscle cells
Adipocytes
Pigment cells
Mesenchymal cells
Undifferentiated cells
Blood & immune cells

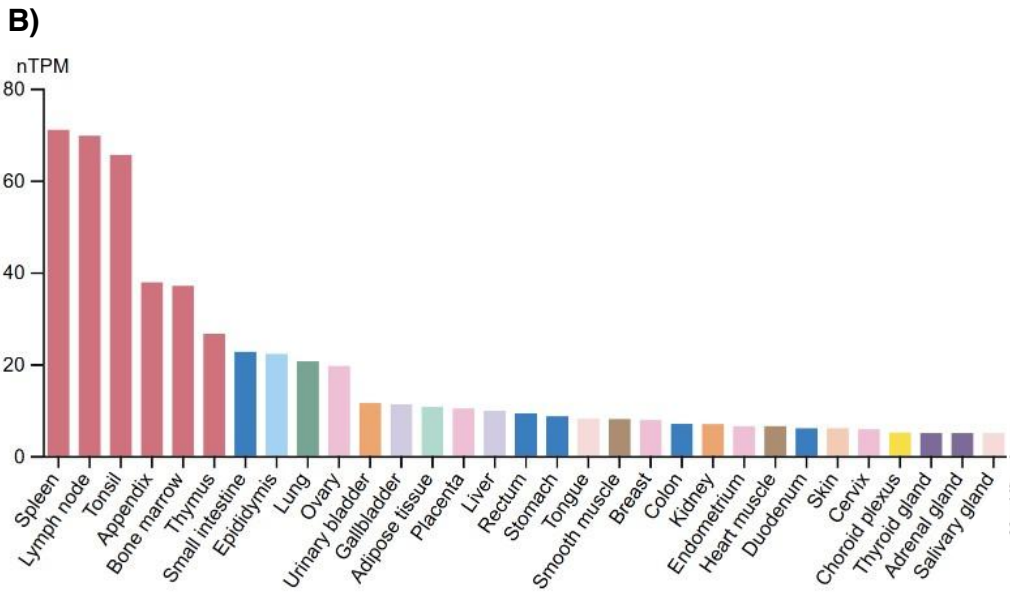

Figure 5. Tissue- and cell-specific ARHGAP25 mRNA expression in humans. *A) Single-cell transcriptomics. T cells, B cells, NK cells, granulocytes, Hofbauer cells, Kupffer cells, and microglia express the highest amounts of ARHGAP25 mRNA. However, excitatory neurons, specific endothelial cells, adipocytes, plasma cells, monocytes, macrophages, dendritic cells, Langerhans cells, and erythroid cells also express ARHGAP25 to a certain degree. B) RNA-seq results of the Consensus dataset (cut-off value: 5 nTPM). High levels of ARHGAP25 were measured in the spleen, the lymph node, the tonsil, the appendix, the bone marrow, and the thymus, suggesting a leukocyte-specific expression. Nonetheless, the small intestine, epididymis, lung, and ovary show moderate ARHGAP25 expression. The charts are taken from The Human Protein Atlas (35, 36).*

1.2.2. ARHGAP25's role in immunity

The potential intracellular function of ARHGAP25 in immune cells was first investigated by Csepanyi-Komi *et al.* (33). Using the PLB-985 cell line differentiated into neutrophil-like cells (dPLB-985) and primary macrophages, they demonstrated that phagocytosis of serum-opsonized yeast cells was significantly elevated in ARHGAP25-deficient dPLB-985 cells, and a similar trend was seen with macrophages. These results indicated that ARHGAP25 might act as a negative regulator during phagocytosis. The work of Schlam and their colleagues on the phagocytosis of macrophages provided further insight into this process. Using primary macrophages and the RAW 264.7 murine macrophage cell line, they provided evidence that ARHGAP25 accumulated at the

phagocytic cups in a PI3K-dependent manner when engulfing IgG-opsonized polystyrene beads of 8.3 μm (37). Overexpression of mCitrine-tagged ARHGAP25 reduced the number of internalized beads. Interestingly, silencing of ARHGAP25 had a similar suppressive effect with beads of 8.3 μm, while uptake of 1.6 μm beads was unaffected. These findings partly complemented those of Csepanyi-Komi but also pointed out the possibility that ARHGAP25 might influence the ingestion of serum-opsonized particles (used by Csepanyi-Komi *et al.*) and the FcγR-mediated phagocytosis (used by Schlam *et al.*) differently (33, 37).

Its role in superoxide production was first revealed by Csepanyi-Komi and their colleagues as well. Silencing ARHGAP25 elevated the superoxide production of dPLB-985 cells upon activation by serum-opsonized zymosan (33). Heat-inactivated serum and PMA showed similar trends but were not statistically different from the ARHGAP25-expressing controls. *In vitro* experiments aiming to unravel the effect of neutrophil-specific GAPs supported these results, as a 10-minute-long incubation with recombinant ARHGAP25 before the induction of NOX2 complex assembly lowered superoxide production, and artificial depletion of ARHGAP25 from neutrophil cell lysate had an opposite effect (38).

Our knowledge about ARHGAP25's role in lymphocyte physiology is still limited. Using an ARHGAP25-deficient (KO) mouse breed, Lindner and their colleagues reported a significant decrease in peripheral CD45+ cell count in KO animals compared to the wild type, which affected both T and B lymphocyte populations (39). Their research, which focused only on uncovering the effect of ARHGAP25-deficiency in B cells, also found a functional alteration in the chemotaxis towards CXCL12. Even though the CXCR4 density of KO and WT B lymphocytes was indistinguishable, KO cells migrated more effectively towards the chemokine. This phenomenon has been previously reported with other cell types (40, 41). *Wang et al.* showed that hematopoietic stem and progenitor cells (HSPCs) of KO mice migrated towards the CXCL12 gradient better (41). *Csepanyi-Komi et al.* observed the same with TNFα-activated bone-marrow-derived neutrophils (40). It is worth mentioning that KO B lymphocytes appeared to be more mobile even without chemokine, whereas this was not the case with HSPCs.

With the use of KO mice, investigating ARHGAP25's possible role in complex immunological processes has been made possible. In one case, K/BxN serum-transfer arthritis—a widely used animal model to simulate the effector phase of rheumatoid arthritis—was induced in KO and WT mice to see if the lack of ARHGAP25 could influence the progression of the disease (42). ARHGAP25 deficiency had an overall protective effect: development of inflammation was less severe with better retained articular functions (measured by horizontal grip test and mechano-nociceptive threshold). Mitigated inflammation was accompanied by decreased synovial hyperplasia, collagen deposition, and cartilage destruction. The dampened inflammation appeared to be due to the reduced accumulation of Ly6G+ and F4/80+ cells in the synovium after K/BxN serum treatment, resulting in lower IL-1β and MIP-2 levels. Western blot-based assessment of the ankle tissue revealed increased MAPK, ERK1/2, IκBα, and E-cadherin levels in WT mice upon K/BxN treatment. ARHGAP25 deficiency caused significantly altered levels of total MAPK and IκBα. Total ERK1/2 and E-cadherin seemed to be also affected, but failed to reach the significance threshold. Additionally, the authors discovered that synovial fibroblasts also express ARHGAP25 (42), which might be a potential contributor to the reported changes, although further experiments are needed to support this idea.

In another study, a different animal model was employed to examine the consequences of ARHGAP25-deficiency on contact hypersensitivity (43). The TNCB-induced (2,4,6-trinitrochlorobenzene) contact hypersensitivity murine model is frequently used for studying allergic contact dermatitis. The disease mechanism comprises two phases, in which keratinocytes and other immune cell types are stimulated, resulting in inflammation of the afflicted skin. The research concentrated on the elicitation phase, which is initiated by the second exposure of the animals to the allergen. Following elicitation with TNCB on the animals' ears, KO mice exhibited reduced ear swelling, akin to KO bone marrow chimeric mice, suggesting that leukocytes mediate the observed effects. The infiltration of leukocytes into the affected skin was less effective in knockout mice, possibly due to variations in the chemokine environment. Nonetheless, the migratory capacity of the KO cells *in vitro* seemed comparable to that of the wild-type cells. The activation of T cells in the lymph nodes following sensitization was evaluated using activation markers (CD69 and CD25). Sensitization elevated the levels of both CD69+ and CD25+ CD4 cells in both knock-out and wild-type T cells, demonstrating no

significant difference during sensitization. Consistent with prior findings, intraocular injection of equivalent cell amounts derived from the lymph nodes of sensitized animals induced similar edema levels in wild-type mice. However, the effect was diminished when an equivalent quantity of WT T-cells was delivered to KO mice. This indicated that the reduced phenotype resulted from the disrupted chemotactic environment in the skin, which inhibited leukocyte migration. (43)

1.2.3. Regulation of ARHGAP25

Just like any other protein, the protein level of ARHGAP25 in a cell can be regulated by influencing its mRNA transcription. Jiang *et al.* showed (44) that higher levels of DNA methylation in the promoter region for the ARHGAP25 gene were accompanied by lower mRNA levels in endothelial cells of the aorta. When seeking to characterize the genetic factors conceivably responsible for elevated eosinophil activation markers (i.e., eosinophil cationic protein and eosinophil-derived neurotoxin) in asthma, Vernet *et al.* found a single-nucleotide polymorphism (rs116571378) (45) that was associated with the methylation level at CpG sites located in the promoter region of ARHGAP25 in eosinophils. However, the function of ARHGAP25 in these cells is still unknown. Interestingly, Csepanyi-Komi *et al.* reported (8) that bacterial stimulus of *S. aureus* reduced ARHGAP25 mRNA and protein levels in human neutrophils.

Phosphorylation is one of the most well-known post-translational modifications, and ARHGAP25 possesses several phosphosites ready to be phosphorylated. When working with HSPCs, Wang and their colleagues found a potential phosphosite, the 363rd serine residue, whose phosphorylation could influence its GAP activity (41). This was the first time a potential regulatory mechanism for the modulation of ARHGAP25's GAP activity was proposed. These findings led to our extensive work led by Eva Wisniewski, who successfully designed an *in vitro* method to follow ARHGAP25's enzymatic activity in a time-dependent manner, with which we could better understand the effect of phosphorylation of different phosphosites on ARHGAP25's enzymatic activity (46). Consequently, we were able to examine the effect of S363, SS379-380, and S488. First, we confirmed that ARHGAP25 can be phosphorylated with the kinases present in a neutrophil cell lysate in a reversible manner. Using phosphorylation-deficient (Ser-to-Ala) mutants, we provided evidence that the phosphorylation of S363 and S488 alone or

together could decrease the protein's GAP activity. Interestingly, the S379-S380 site appeared to have a modulatory role when combined with S363, as it diminished the observed changes (46). These results showed a glimpse of a complex regulatory mechanism that could influence RAC-mediated processes through ARHGAP25.

1.2.4. ARHGAP25's role in cancer development

ARHGAP25's potential in cancer research has received growing interest in the previous years, as ARHGAP25 mRNA levels differ between healthy and tumorous tissues in several cancer types (47). However, leukocytes migrating toward the tumor tissue can greatly influence the overall ARHGAP25 expression (measured by bulk RNAseq of the tissue), which creates a challenging task to differentiate between tumor- and immune-related effects. Moreover, cancer research is unfortunately a hotspot for paper mills and, consequently, fraudulent articles (48). Some ARHGAP25-related articles have already received concerns about their integrity, which have not been resolved (depicted in Figure 6), so those articles were excluded from the following summary (49).

Considering its involvement in leukocyte physiology, ARHGAP25's potential role in immune cell-derived tumors is anticipated. Although one article reported three instances of high-confidence loss-of-function mutations (S495P, Y129M, M90H) in large granular lymphocyte leukemia and a generally lower ARHGAP25 mRNA level in AML and ALL patients (compared to healthy individuals), there is no further evidence of ARHGAP25 playing a key role in these tumor progressions (50).

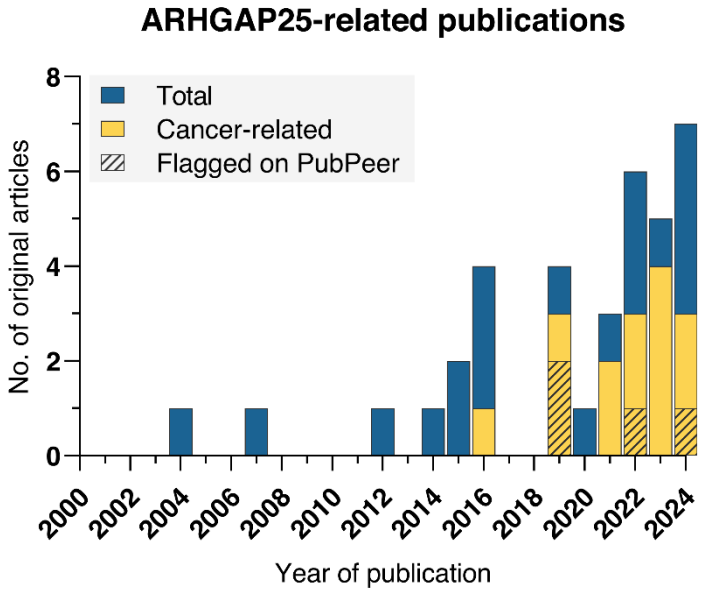

Figure 6. Timeline of the ARHGAP25-related publications. *The number of original articles available on PubMed that contain the search word 'ARHGAP25' is collected. Of the 32 articles, 16 are connected to cancer research. However, serious questions about the integrity of the results were raised on PubPeer in four cases. The figure is created by the author based on the search result of "ARHGAP25" on PubMed (www.pubmed.ncbi.nlm.nih.gov) and PubPeer.*

In 2016, Thuault *et al.* reported an interesting trend when searching for molecular differences between rhabdomyosarcoma subtypes (51). Alveolar rhabdomyosarcoma (ARMS), which is identified by the PAX3-FOXO1A or PAX7-FOXO1A chimeric oncogenic transcription factor, was associated with a high risk of metastasis compared to ERMS (embryonic rhabdomyosarcoma) (52). ARMS cells showed increased invasion potential and a more circular cell shape in their experiments. This increased invasion could be inhibited by a Rho GTPase inhibitor (exoenzyme C3 transferase) and Rho kinase (ROCK) inhibitors (Y27632 and H1152). They achieved even better inhibition by silencing ROCKII, whereas ROCKI inhibition was ineffective. Unlike ARHGAP24 and ARHGAP22, which were inconsistently expressed among RMS cell lines, ARHGAP25 was undetectable in ERMS cell lines, while ARMS cells showed a generally upregulated ARHGAP25 (specifically 'Isoform C') expression. Silencing ARHGAP25 in an ARMS cell line with high expression (namely Rh4) decreased its invasive potential. Moreover, similar results could be achieved by transfecting the cells with the R193A mutant, which

also increased cell spreading and RAC1 activity, indicating that this mutant acted as a dominant negative towards endogenous ARHGAP25. ARHGAP25 overexpression in an ERMS cell line (namely RD) increased its cell spreading, while that of the R193A mutant had no effect. Interestingly, when ROCKII-silenced Rh4 cells were transfected with ARHGAP25 R193A, the increased cell spreading (caused by ROCKII-deficiency) returned to a level similar to ROCKII-expressing Rh4 cells.

ARHGAP25 mRNA levels are reportedly lower in breast tumor tissues than in healthy ones (53). Han *et al.* investigated how altering ARHGAP25 expression in breast adenocarcinoma cell lines (namely T-47D and SK-BR-3) could affect their tumor functions (53). Overexpression of ARHGAP25 decreased the proliferation, migration, and invasive capacity of the cells *in vitro*, as well as tumor growth in a xenograft model. In contrast, silencing ARHGAP25 achieved the opposite results. Based on their rigorous studies regarding ARHGAP25's effect on molecular mechanisms, they proposed that ARHGAP25 affected transcription of proliferation and migration-associated genes via RAC1 inhibition. Moreover, they revealed that ASCL2, one of the downstream targets of ARHGAP25, inhibited the transcription of ARHGAP25. Complementing the former results, Müller *et al.* reported (54) that ARHGAP25 was significantly associated with low metastatic potential (HR: 0.7 [0.6–0.9]; p value: 3.8×10^{-5}) in breast cancer. A similar favorable prognosis was associated with ARHGAP25 expression in the case of colon carcinoma (55).

In the case of pancreatic adenocarcinoma, a similar overall picture was observed. The tumor size and the tumor stage correlated with ARHGAP25 expression (56). Huang *et al.* demonstrated (56) that ARHGAP25 was decreased in cancer cell lines (namely PANC-1, SW1990, BxPC-3, Capan-1, AsPC-1) compared to HPNE, an immortalized pancreatic cell line. The authors generated an ARHGAP25-overexpressing AsPC-1 and two ARHGAP25-silenced BxPC-3 lines to investigate the effects of the protein expression on tumor functions. Overexpression decreased proliferation, tumor volume, and weight, while the opposite was observed in silenced cells. Silencing also attenuated the cytotoxic effects of gemcitabine and 5-fluorouracil. Overexpression decreased phospho-Akt, phospho-MTOR, phospho-PAK1, as well as HIF1α, which could influence glucose transporter upregulation and glycolysis (via *e.g.,* PKM2 and LDHA, which were also reduced). Consequently, it reduced glucose uptake, extracellular lactate levels, and

intracellular ATP. As silencing had the opposite effect on the mentioned protein, lactate, ATP levels, and glucose uptake, the authors treated the cells with a PI3K and mTOR inhibitor (PF-04691502), which abolished the changes in protein phosphorylation, glucose uptake, lactate, and ATP levels.

1.3. Protein-protein interactions

1.3.1. Experimental methods

Protein-protein interactions (PPIs) are indispensable elements of intracellular signaling. A typical cell contains millions of proteins confined in a space less than a picoliter (57). This dense milieu forces proteins to meet frequently, resulting in countless transient protein associations or, in some instances, the assembly of protein complexes. These interactions lead to signal transmission via conformational changes or possible biochemical events, resulting in protein activation, inhibition, or translocation (58). Due to its complexity, PPI identification is a challenging endeavor. However, our tools have become increasingly sophisticated, and new methodologies have emerged to investigate the formation of PPIs. Still, despite the significant advancements in this field, there is no superior alternative among the methods, as they all have specific advantages and downsides (59).

One of the most conventional methods is the ‘yeast two-hybrid' (Y2H) assay, which allows the identification of pairwise PPIs. It provides an *in vivo* approach to detect physical direct interaction using the yeast transcription factor Gal4 and a selective reporter (*e.g.,* His3) (60). Two artificial protein constructs are created by fusing the candidates to the Gal4 DNA-binding and activation domains, respectively. Then, the plasmids coding the constructs are transfected into the yeast. Transcription of the reporter gene occurs only during the interaction between the two candidates. Although only one interaction can be confirmed at a time with this approach, the workflow has allowed upscaling the method in a high-throughput manner (61). Nonetheless, its limitations have rendered the method fairly outdated. Using yeast as a host system fails to incorporate mammalian-specific post-translational modifications (60). Moreover, they are prone to producing a high percentage of false-negative and, without the appropriate negative controls, false-positive results. To overcome certain limitations of the model, several Y2H variants have emerged, but none of them could resolve all of its setbacks (60).

Affinity purification-coupled mass spectrometry (AP-MS) provides an opportunity to detect stable interactions between the target protein (bait) and any interacting candidate(s) (prey). This process—usually called a *pulldown*—requires the tagged protein to be captured by the tag-specific motifs-containing resin and a protein pool with the potential candidates (62). If the interactions between the bait and the prey molecules are strong enough, they remain bound together on the surface of the resin, while the less stable, nonspecific associations are rinsed off during the washing steps. The associated proteins can later be eluted from the resin and then analyzed by mass spectrometry (62). The major disadvantage of the method lies in the use of molecular tags, which can introduce false positive interactions, alter the natural folding of the bait protein, mask interaction sites, *etc*. (62). Using protein-specific antibodies to capture the endogenous bait protein (called *immunoprecipitation*) bypasses these problems, although at the cost of worse signal-to-noise ratios (62). Crosslinking of the formed protein associations can help identify less stable interactions, but doing so increases the complexity of the identification (63). Even though detection of the eluted proteins can be achieved by more commonly available methods (e.g., Western blot), using mass spectrometry allows the identification of all the constituents of the eluate. Quantification of the eluted proteins may be accomplished via labeling of the eluates, although nowadays, several label-free approaches exist for MS quantification (64).

In vivo label transfer assays have gained increased popularity over the years as they reveal the interactions in their natural environment. The method usually requires a small molecule (e.g., biotin in the case of *BioID*) that can be attached to the target molecules (65). This requires specifically tailored enzymes that can modify any surrounding proteins. If such a promiscuous protein is fused to and co-expressed with the bait, all proteins surrounding the bait can be labeled *in vivo* and identified (65). However, the fused protein construct might behave differently in the cell than the endogenous form, and labeling enormous numbers of proteins can disturb the homeostasis of the cell (65, 66).

Resorting to microscopic imaging is a common approach when it comes to PPI detection. The basic concept of co-localization is simple: if you stain the cell with bait- and prey-specific, fluorophore-tagged antibodies, an overlap of the two fluorophores at the site could indicate protein interaction. However, closeness does not always mean

interaction: the odds of two proteins being in close proximity in a cell are pretty high (67). Moreover, the specificity of the antibodies, the characteristics of the fluorophore, and the microscope's resolution should also be considered as potential limitations (67). However, the *proximity ligation assay (PLA)* provides a more sophisticated approach (68). Two specifically tailored secondary antibodies are used (PLA probes) that have a short sequence-specific DNA strand attached to them. These probes can recognize the bait- and prey-specific primary antibodies. If the two probes are in close proximity due to the interaction of the bait and the prey (and other components, *e.g.,* sequence-specific DNA oligonucleotides, appropriate substrates, and enzymes, are provided), rolling cycle replication occurs at the site of the interaction, resulting in great amplification of the DNA circle. When viewed with a fluorescence microscope, the amplified DNA can be visualized with fluorescent complementary oligonucleotide probes that bind to the amplified DNA. This method also provides an opportunity to gather specific information about the intracellular placement of the interaction.

Fluorescence resonance energy transfer-based (FRET) or bioluminescence resonance energy transfer-based (BRET) assays provide *in vitro* and *in vivo* alternatives for PPI detection. Both methods require energy transfer between the donor and the acceptor molecules that can be fused to the bait and the prey proteins to investigate their interaction. FRET uses a donor dye (*e.g.,* CFP) that, when excited by laser beams, can transfer some of its energy to the acceptor molecule (*e.g.,* YFP), resulting in fluorescence emission at a characteristic wavelength (69). Co-expression of fusion constructs in living cells enables their interaction to be studied quantitatively in real-time since the acceptor's emission depends on the donor's proximity. The fact that external illumination of the donor molecule is essential for the energy transfer limits the use of FRET, as direct excitation could raise background noise or cause photobleaching (70). However, BRET uses a luciferase enzyme as a donor to excite the acceptor. As the donor does not require prior excitation, the results have a low background, and most problems associated with FRET are limited (*e.g.,* autofluorescence, light scattering, or photobleaching) (69, 70).

In silico approaches to simulate and predict PPI formations are blooming. We have achieved major advancements in protein structure prediction, and their precision in PPI prediction is increasing yearly (71). Numerous prediction tools currently exist that can predict PPIs using only the amino acid sequence of the proteins (71, 72). Most recent

releases can integrate PTMs and small molecules into the prediction (73). However, the need to validate these findings is still indispensable (74).

1.3.2. ARHGAP25's interaction profile

Mapping the interactome of small GTPases and their regulators has received interest in cellular biology due to their relevance in inflammatory diseases and cancer (75-79). Bagci *et al.* (76) generated a comprehensive library using proximity labeling to identify the interactome of Rho-family GTPase members. They used wild-type and mutant small GTPases as baits expressed in HEK293 and HeLa cells. Although their findings provide the most profound Rho-family proteome, the choice of these cell lines restricted the identification of PPIs with non-ubiquitous proteins (including ARHGAP25).

Müller *et al.* (78) followed a different approach to investigate the same proteome. They used tagged RhoGAPs and GEFs as baits expressed in HEK293T cells to perform AP-MS Although they included ARHGAP25 in their experiments ('Isoform 3'), their experiments failed to replicate its RAC-specificity, which raises concerns about the used construct. Moreover, they also missed the opportunity to investigate cell-specific interactions. The list of ARHGAP25's partners reported in the article is provided in Table 1.

The BioGRID database—a biomedical interaction repository with data compiled through comprehensive curation efforts—currently contains 49 interactors associated with ARHGAP25.(80) They are collected from the data provided by Müller et al. and the one created throughout the BioPlex ('Biophysical Interactions of ORFeome-derived Complexes') projects (81-83).

Table 1. The list of interaction partners of ARHGAP25 identified by Müller et al. *The list is collected from the referenced article (78) by the author.*

Gene name	Protein name
CAMK2D, CAMK2G	Calcium/calmodulin-dependent protein kinase type II (subunit δ/γ)
CDKN2A	Cyclin-dependent kinase inhibitor 2A
MAT2A, MAT2B	S-adenosylmethionine synthase subunit α/β
MTCH2	Mitochondrial carrier homolog 2
ALDH18A1	Delta-1-pyrroline-5-carboxylate synthase
CKAP4	Cytoskeleton-associated protein 4
EIF6	Eukaryotic translation initiation factor 6
LANCL1	Glutathione S-transferase LANCL1
LGALS3BP	Galectin-3-binding protein
POTEE	POTE ankyrin domain family member E
PPM1G	Protein phosphatase 1G
PPP1R9B	Neurabin-2
PPP2R1A	Serine/threonine-protein phosphatase 2A
PRDX4	Peroxiredoxin-4
PSMA1	Proteasome subunit α type-1
HACD3	3-hydroxyacyl-CoA dehydratase 3
UBA1	Ubiquitin-like modifier-activating enzyme 1
XPO1	Exportin-1

The latter project applied high-throughput AP-MS to identify PPIs of C-terminally tagged baits in HEK293T cells. By the 3rd iteration of the project, called BioPlex 3.0 (81), they have identified more than 56 thousand interactions between 10 thousand proteins (half the human proteome). ARHGAP25 was also included as bait in these studies, resulting in several identified interactions (refer to Table 2). However, as mentioned previously, ARHGAP25 is not endogenously expressed in HEK cells, so no other baits were associated with ARHGAP25 as prey.

Table 2. Interaction partners of ARHGAP25, identified via the BioPlex projects. *The 'x' marks the iteration (BioPlex 1.0-3.0) when the given protein was listed as an interaction partner for ARHGAP25. The list is collected from the* BioGRID database *(81-83) by the author.*

Gene name	Protein name	BioPlex		
		1.0	2.0	3.0
ACACA	Acetyl-CoA carboxylase α	x		
ANGEL1	Protein angel homolog 1	x		
AP5B1	Adaptor-related protein complex 5 β subunit	x	x	
ATG7	Ubiquitin-like modifier-activating enzyme ATG7	x	x	x
C2ORF44	WD repeat and coiled-coil-containing protein	x		
CAMK2D, CAMK2G	Calcium/calmodulin-dependent protein kinase II δ/γ	x		
DDX11L8	Putative ATP-dependent DNA helicase DDX11-like protein 8	x		
DMWD	Dystrophia myotonica WD repeat-containing protein	x	x	x
DPP9	Dipeptidyl-peptidase 9	x		
DPYSL4	Dihydropyrimidinase-related protein 4	x		
DSTYK	Dual serine/threonine and tyrosine protein kinase	x	x	x
DYNC2H1	Cytoplasmic dynein 2 heavy chain 1	x		
GTF2H2	General transcription factor IIH subunit 2	x		
HERC3	Probable E3 ubiquitin-protein ligase HERC3	x		
KDM5C	Lysine-specific demethylase 5C	x	x	x
MSTO1	Misato1, mitochondrial distribution and morphology regulator	x	x	x
NPRL3	Nitrogen permease regulator 3-like protein	x		
PER1	Period circadian clock 1	x	x	x
POLD1	DNA polymerase δ catalytic subunit	x		
RECQL4	ATP-dependent DNA helicase Q4	x	x	x
SEC23IP	SEC23-interacting protein	x	x	
TBL3	Transducin β-like protein 3	x	x	x
THUMPD3	tRNA (guanine(6)-N(2)) -methyltransferase	x		
TRIM27	Zinc finger protein RFP	x		
TRIM65	E3 ubiquitin-protein ligase TRIM65	x		x
UBA6	Ubiquitin-like modifier activating enzyme 6	x	x	x
VWA9	Von Willebrand factor A domain-containing protein 9	x		
WRAP53	Telomerase Cajal body protein 1		x	

2. Objectives

There is an increasing number of ARHGAP25-related articles from different fields of science where the underlying molecular mechanisms remain obscure. In this current thesis, we would like to use different methodologies to find regulators and other interaction partners that partake in ARHGAP25-mediated processes to widen our understanding of small GTPase regulation in neutrophils. To this end, we wish to investigate whether the overexpression of Ser-to-Ala phospho-mutants, which behaved differently in our Rac-specific GAP assay *in vitro*, may affect intracellular processes. As the protein is highly specific to leukocytes, which are known to express a wide range of other cell-specific macromolecules, we wish to extend the currently available ARHGAP25 proteome via data gathered from neutrophil-specific PPI experiments to see if we discover new, previously unreported interactions.

The current aims are as follows:

I. Investigation of the effects of the ARHGAP25 Ser-to-Ala phospho-mutants on total and active RAC levels and the related actin reorganization via the F-actin content.
II. Creation of a neutrophil-specific interactome via GST-pulldown and co-immunoprecipitation and subsequent investigation of the proteome via bioinformatic approaches to shed light on potential protein partners and related molecular functions.
III. Investigation of the identified small GTPase partners and potential phosphorylation-related interactions of ARHGAP25.

3. Methods

3.1. Creation of the plasmid constructs and corresponding cell lines

ARHGAP25 was extracted from the cDNA of human peripheral blood leukocytes (’Isoform 4’) and cloned into the pcDNA3.1/V5-His-TOPO vector. A plasmid containing the LacZ gene was used as the negative control. These plasmids carry an antibiotic resistance gene providing the selection of the transfected cells with geneticin (G18). Mutations were introduced via site-directed mutagenesis using specific primers (Table 3) and confirmed by Sanger sequencing [Microsynth AG].

Table 3. Primer pairs used for the site-directed mutagenesis.

	Primer pairs (5’ to 3’ direction)	
S363A	forward	CCCTGGCACCCCCTGCCCAGAAAAATGACC
	reverse	CAGGGGGTGCCAGGGGTATATCCTTGGACTTGG
S379-380A	forward	CCCGAGCCGCTGT AGGCTGGGATGCCACTG
	reverse	GCCTACAGCGGCTCGGGCCACTGGAGCTTTCTTGG
S488A	forward	ACGATGGCTCAAGACTTGCGCCAACTTTCTG
	reverse	GTCTTGAGCCATCGTTCTCCTGTGCCCTTCC

PLB-985 cells were grown in RPMI-1640 medium (supplemented with FBS [10%], penicillin [50 units/mL], and streptomycin [50 µg/mL]) and grown in a 5% humidified CO_2 incubator at 37 °C.

The cells were transfected via electroporation with an Amaxa Nucleofector™ in accordance with the manufacturer's guidelines. The cells were initially serum-starved in UltraMEM medium devoid of FBS or antibiotics for one hour. The previously described plasmids were transfected into the cells, and the cells were incubated in UltraMEM for 2 hours before transferred to the selective medium (the aforementioned supplemented RPMI-1640 containing an additional 1 µg/mL geneticin). The cells were cultivated in this selective medium for a minimum of three weeks prior to use. Transfected PLB-985 cells were differentiated into neutrophil-like cells for 7 days using 0.5% dimethylformamide.

3.2. Measurement of active RAC content and Western blotting

Cells were lysed in a cell lysis buffer (composed of 50 mM Tris–HCl, 100 mM NaCl, 2 mM $MgCl_2$, 10% (v/v) glycerol, 1% Nonidet P-40 (IGEPAL CA 630), 1% (v/v)

aprotinin, 1% (v/v) ‘Phosphatase Inhibitor Cocktail 2,’ 1% (v/v) ‘Protease Inhibitor Cocktail,’ and 1 mM PMSF) for 5 minutes on ice. The supernatant was isolated via centrifugation (16,000 g, 5 minutes, 4 °C). GTP-bound RAC was extracted from the supernatant utilizing the GTPase-binding domain of p21-activated kinase (PAK-PBD) fused to GST (provided by Prof. T. Wieland). The protein content of the cell lysate was measured (according to Bradford), diluted to equal concentrations, and incubated with the beads for 50 minutes at 5 °C. After washing three times with 0.1% Nonidet P-40-containing PBS, resin-bound proteins were eluted in 1 × Laemmli Sample Buffer at 95 °C for 5 minutes. To measure the total RAC content of the cells, cell lysates with equal protein masses were heated at 95 °C for 5 minutes in 1 × Laemmli Sample Buffer.

Equal volumes of the cell lysate samples, along with ProSieve QuadColor Protein Marker, were loaded into gradient polyacrylamide gels for electrophoresis. Following separation, proteins were transferred to nitrocellulose membranes and subsequently stained with Ponceau solution. Blocking was performed for 15 minutes in EveryBlot blocking buffer, followed by overnight incubation with RAC-specific primary antibody [cat. no: 2465; Cell Signaling Technology®] at a 1:1000 dilution at 4 °C. Bound antibodies were identified via enhanced chemiluminescence using horseradish peroxidase-conjugated anti-rabbit secondary antibody at a 1:5000 dilution for 1 hour at room temperature. GAPDH served as a loading control for these measurements. Active RAC content was determined similarly, but using equal volumes of the eluted samples.

We performed a densitometric analysis of the acquired X-ray films using the ImageJ software. Independent measurements were normalized to the ‘Vector.’ We determined the total RAC content of the cells by the $log_2 \frac{RAC_{total}}{GAPDH}$ calculation and the active RAC ratios by $log_2 \frac{RAC_{active}}{RAC_{total}}$. The individual or combined effect of the introduced mutations at the different positions was evaluated using three-way ANOVA, and multiple comparisons were assessed between the ‘WT’ and the other groups using Dunnett’s multiple comparisons test.

3.3. Actin staining of PLB-985 cells

2×10^6 differentiated PLB-985 cells were fixed with 4% paraformaldehyde for 15 min at room temperature and permeabilized with PBS containing 0.1% Tween-20

(PBST) for 5 minutes at room temperature. Alexa fluor-488 conjugated phalloidin was used to stain F-actin (1:100 dilution) for 20 minutes at room temperature. Washing steps with PBS were included between each step. Ten thousand cells were measured using a CytoFLEX flow cytometer, and the median fluorescence intensities (MFI) were compared. The individual or combined effect of the mutations at different positions was evaluated using three-way ANOVA, and multiple comparisons were assessed between the 'WT' and the other groups using Dunnett's multiple comparisons test.

3.4. Isolation and cell lysis of human neutrophilic granulocytes from peripheral blood

We used the buffy coat from healthy adult male volunteers (in the case of GST-pulldown) and the peripheral blood taken from healthy volunteers (in the case of co-immunoprecipitation) to isolate neutrophils, approved by the Department of Health Administration of the National Public Health Center of Hungary (31937-7/2020/EÜIG). Dextran sedimentation procedure followed by Ficoll-Paque gradient centrifugation was utilized to separate neutrophils as described previously (84). Each batch was aliquoted into portions containing 40 million cells, snap-frozen in liquid nitrogen, and stored at –80 °C until further use.

Frozen neutrophil pellets were resuspended in ice-cold cell lysis buffer (as described in section 3.2) and lysed on ice for five minutes. The supernatant was separated from the pellet via centrifugation and divided into four equal portions. Two portions remained intact, while two aliquots were subjected to pretreatment with 15 mM EDTA and either 15 mM GTPγS or 10 mM GDPβS for 15 minutes at room temperature with agitation at 250 rpm to enrich the active and inactive forms of the GTPases. Subsequently, the samples were placed on ice, and a $MgCl_2$ solution was added to achieve a final concentration of 60 mM to terminate the reaction.

3.5. Preparation and pulldown of GST-fused recombinant proteins

GST and full-length GST-coupled ARHGAP25 were synthesized in *E. coli* (strain: One Shot™ BL21 Star™). First, bacteria transfected with the plasmids were incubated overnight in a lysogeny broth medium supplemented with 100 µg/mL ampicillin. IPTG was administered to the medium 3 hours prior to harvest to induce protein expression. Bacteria were removed from the medium using centrifugation and subsequently lysed with sonication in a lysis solution. Insoluble cellular debris was eliminated during

centrifugation, and the recombinant proteins were purified using glutathione-bound beads. Protein-coated beads were washed thrice, and aliquots were preserved at –80 °C for future use.

GST-ARHGAP25 and GST-coated beads were incubated with cell lysates for 45 minutes at 4 °C. Beads were separated using centrifugation and rinsed three times with PBST. Protein elution was performed by boiling the beads at 95 °C for 5 minutes in 30 µL of 2 × Laemmli buffer, and the elution was kept at –20 °C.

3.6. Co-immunoprecipitation

Protein A magnetic beads [Miltenyi Biotec] were coated with either polyclonal ARHGAP25 antibody (created and tested by our group) or rabbit IgG [cat. no: I5006; Sigma Aldrich] and incubated with intact total cell lysate for 45 min at 4 °C. Beads were separated from the supernatant by magnetic force and washed three times with PBST. Bound proteins were eluted by boiling the beads (at 95 °C for 5 min) in 30 µL 2 × Laemmli buffer. Eluted samples were stored at −20°C until analysis.

3.7. Sample preparation for proteomics

We performed gel-aided sample preparation on all samples as previously described (85). Samples were reduced with 10 mM DTT, alkylated with 22 mM iodoacetamide, and digested with trypsin. The mixtures were acidified, and $\frac{1}{8}^{th}$ of the samples were placed in a single-use Evotip trapping mini-column. Data-dependent LC-MS/MS analysis utilized an Evosep One stainless steel emitter (ID 30 µm) linked to a linear ion trap-Orbitrap (Orbitrap-Fusion Lumos, Thermo Fisher Scientific) mass spectrometer functioning in positive ion mode. During data acquisition, multiple charged ions were selected in a cycle time from each MS survey scan for ion-trap HCD fragmentation. MS spectra were obtained in the Orbitrap (R = 60,000), and MSMS were conducted in the ion trap.

3.8. Label-free quantification

Following the conversion of raw files to .mzML format using MSConvert (v. 3.0) for compatibility, we employed the ‘LFQ-MBR’ workflow of the FragPipe program (FragPipe v. 19.1, MSFragger v. 3.7, IonQuant v. 1.8.10, Philosopher v. 4.8.1) for data analysis. The precursor and fragment mass tolerance was set to ± 5 ppm and 0.6 Da, respectively, while other database search parameters and identification acceptance criteria

remained in default settings. A human proteome database, including decoys and contaminants, was downloaded via FragPipe (accession date: 27th May 2023) and manually supplemented with the GST-tag sequence (Uniprot ID: P08515). IonQuant LFQ was selected with the 'MBR top runs' parameter configured to 25. The generated raw and processed data are available as supplement material online (86). Raw data was obtained from the 'CombinedProtein.tsv' file (generated by the FragPipe software) through the FragPipe Analyst web application (87). The 'MaxLFQ' intensity values for each sample were subjected to $\log_2$ transformation. Samples were grouped by conditions and went through filtering (filtering criteria: 'Minimum percentage of non-missing values globally' = 0, 'Minimum percentage of non-missing values in at least one condition' = 60). The 'Missing Not At Random' (MNAR) imputation approach employed random samples from a left-shifted Gaussian distribution of 1.8 standard deviations apart with a width of 0.3 to address missing values and introduce noise for subsequent analysis. Additional parameters: Normalization method: Variance stabilizing normalization.

3.9. Data evaluation of the GST pulldown samples

In the case of processed data, corresponding to the GST-pulldown measurements, protein-wise linear models combined with empirical Bayes statistics were employed for the differential expression analysis via the FragPipe Analyst web application (87). The limma package from the R Bioconductor created a list of differentially expressed proteins for each pairwise comparison. A threshold of the adjusted p-value of 0.05 (Benjamini–Hochberg method) and a fold change (FC) have been utilized to identify significantly regulated proteins in each comparison. Fold change was calculated as follows: $FC = \frac{LFQ_{GST-ARHGAP25}}{LFQ_{GST}}$.

3.10. Data evaluation of the co-immunoprecipitation samples

For processed data corresponding to the co-immunoprecipitation measurements, we employed a score-based evaluation to determine the presence and relative abundance of previously identified potential partners. Proteins were categorized into three groups based on their detection rates in the co-IP samples: 'low' (< 60%), 'good' (60% to 80%), and 'excellent' (> 80%), creating the 'confidence score' metric. Proteins were assigned an 'enrichment score' according to their $\log_2$ fold change ($\log_2$FC) value (where $FC = \frac{LFQ_{ARHGAP25}}{LFQ_{control}}$) relative to the median $\log_2$FC ('low': FC < 0.81 and 'high': FC > 0.81). Based

on these parameters, each protein was classified into four categories: 'unlikely,' 'low credibility,' 'satisfactory,' and 'high credibility.' The steps for the evaluation are available online (86).

3.11. Reassessment of MS results using Western Blot

Equal volumes of eluates from GST-pulldown samples, along with ProSieve QuadColor Protein Marker, were processed as described in section 3.2. The primary antibodies against SYK [cat no: sc-1240; Santa Cruz], ACSL1 [cat no: 4047S; Cell Signaling Technology®], LDHA [cat no: 2012S; Cell Signaling Technology®], RHOG [cat no: E9B7Z; Cell Signaling Technology®], RAC2 [cat no: PA5-29681; Invitrogen], and RAB27A [cat no: MAB7245; Bio-Techne] were used to visualize their presence or absence in a qualitative manner.

3.12. Functional enrichment analysis

Functional enrichment analysis was conducted via the ShinyGO web server (v. 0.8041) (88). The user threshold was established at 0.01 for the “Gene Ontology (GO) biological process” and “Reactome” data sources, filtered by term size (minimum: 5, maximum: 1000). A neutrophil-specific background of human origin (89) was included to eliminate false positive results.

3.13. STRING analysis

The STRING platform (v. 12.043) was utilized to gather all recorded physical interactions among our prospective protein partners determined by MS (90). Only experimentally determined interactions and databases were included to achieve a more robust network acquisition. The computer allocated a score ranging from 0 to 1 to each interaction, reflecting the robustness of evidence supporting the interaction. A threshold of 0.400 was utilized to exclude less likely interactions. Proteins lacking identified interactions were omitted. The acquired network was imported into Cytoscape (v. 3.10.1.44) for data visualization. Physical interactions are illustrated by edges connecting proteins, denoted by nodes.

3.14. In silico PPI prediction

The direct interaction formation of ARHGAP25 and likely partners was predicted in silico using AlphaFold optimized for multimers.(72, 91) The primary settings were as follows: num_relax: 0; template_mode: none; msa_mode: mmseqs2_uniref_env;

pair_mode: paired; model_type: AlphaFold2_multimer_v3; num_recycles: 20; recycle_early_stop_tolerance: 0.5; relax_max_iterations: 200; pairing strategy: greedy; max_msa: auto; num_seeds: 2.

Dimers comprising fewer than 500 amino acids were generated using ColabFold (v1.5.545). In contrast, multimers with a cumulative total exceeding 500 amino acids were processed by Neurosnap Inc. (Computational Biology Platform for Research, Wilmington, DE, 2022 https://neurosnap.ai/) due to substantial computational demands. The predicted dimer was rendered in ChimeraX.

3.15. In silico prediction of 14-3-3 binding phosphosites

We utilized an improved prediction web interface developed by Madeira *et al.*, following the authors' guidelines (92). The algorithm evaluates each phosphosite based on three distinct parameters and highlights those with an increased probability of serving as binding sites for 14-3-3 proteins. The generated data are available as supplement material online (86).

3.16. Phosphorylation of GST-coupled proteins

The phosphorylation was carried out in a solution containing 500 µL of cytosolic extract from primary human neutrophils (as described in section 3.4) in the presence of 30 µL kinase buffer (20 mM Tris–HCl, pH = 7.4, 10 mM $MgCl_2$, 0.1 mM Na-EGTA, 1 mM dithiothreitol [DTT], 1% Phosphatase Inhibitor Cocktail 2, 1% Protease Inhibitor Cocktail, 1 mM PMSF, and 1 mM adenosine 5′-triphosphate [ATP]) for 30 min at 30 °C.

3.17. Statistics

Graphs were generated using GraphPad Prism (v. 10.2.0). Each statistical test and its corresponding significance thresholds were selected based on the data characteristics and are clarified in the related method section and figure legend. The default significance threshold was set to 5%.

4. Results

4.1. Creation of PLB-985 cells expressing the ARHGAP25 Ser-to-Ala mutants

To investigate the effects of the overexpression of phospho-deficient ARHGAP25 mutants *in vivo*, we constructed DNA plasmids encoding Ser-to-Ala mutants of ARHGAP25 targeting four serine residues at three positions (S363, S379-380, and S488) individually and in combination, creating seven experimental groups (S363A, S379-380A, S488A, S363A+S379-380A, S363A+S488A, S379-380A+S488A and S363A+S379-380A+S488A [referred to as: TM]), along with the LacZ-expressing negative control ('Vector') and the wild-type ARHGAP25-coding vector (WT). The vectors were transfected into PLB-985 cells, after which stable vector-expressing cells were generated and differentiated into neutrophil-like cells as outlined in the 'Methods' section. The successful plasmid expression was evaluated by Western blot (Figure 7).

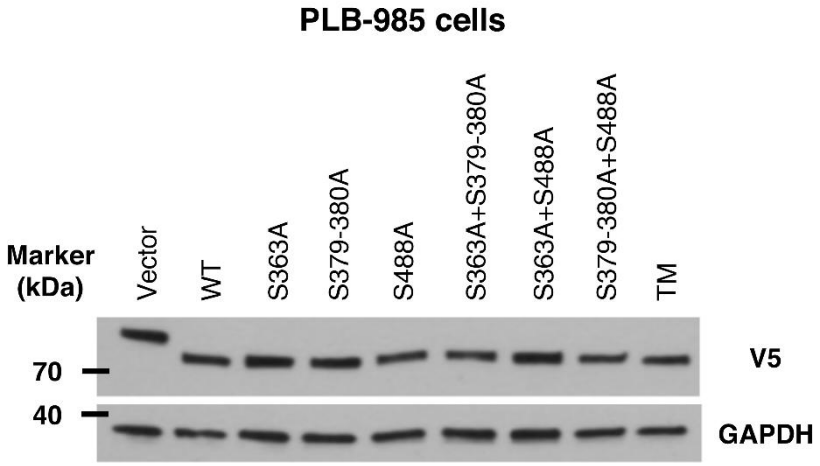

Figure 7. Evaluation of the expression of the transfected proteins in PLB-985 cells. *Cells were differentiated for 7 days, collected, and lysed in a lysis buffer. Protein content was equalized among the samples before electrophoresis. Anti-V5 (cat. no: MCA1360; BioRad) and anti-GAPDH (cat. no: 2118; Cell Signaling Technology®) antibodies were used to detect the protein constructs and the housekeeping protein. All V5-tagged proteins were detected in the samples with no apparent difference in protein expression. The band corresponding to the vector (V5-tagged β-galactosidase) appeared at approximately 120 kDa. The figure is based on our own published data, redesigned to fit the thesis (46).*

4.2. The effect of ARHGAP25 Ser-to-Ala mutants on the total and GTP-bound RAC levels in PLB985 cells

The total RAC content of the cell lysates was assessed via densitometric analysis of the Western blots. A pan-RAC-specific antibody was employed to assess its levels in relation to GAPDH. The $\frac{RAC_{total}}{GAPDH}$ ratios were normalized to the control 'Vector' and logarithmically transformed. Figure 8 illustrates the outcome of four independent measurements. Based on the three-way ANOVA, the biggest source of variation was caused by the introduction of the S379-380A mutation, but it did not reach significance (p=0.069). The most prominent difference was observed between the WT and the S379-380A+S488A double mutant-expressing groups, yet it failed to reach the significance threshold (p=0.081).

The amount of RAC-GTP was assessed via pulldown using PAK-PDB-GST-coated beads as bait. The eluted RAC-GTP levels were compared to the total RAC levels using Western blot in a similar fashion as described previously. There was a considerable amount of variation present among the independent pulldowns. The three-way ANOVA identified the interaction of the three mutations as the most prominent source of variation (12.8%), yet it failed to reach significance (p=0.064), and there was no significant difference between the 'WT' and the other groups.

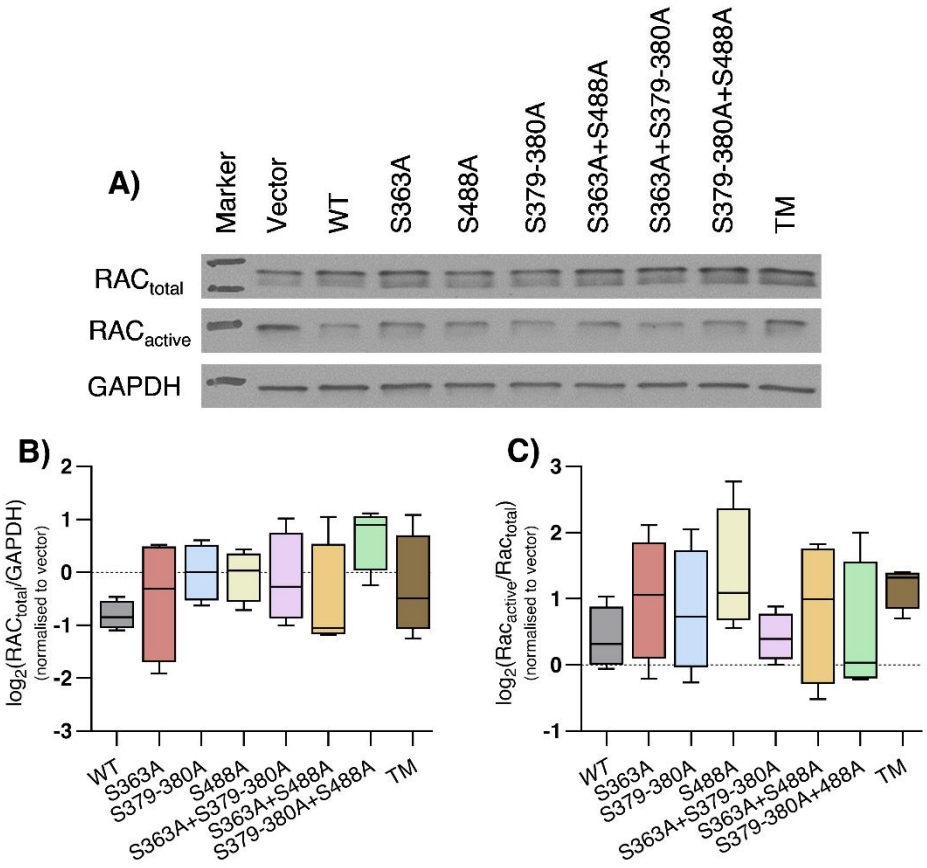

Figure 8. The effect of overexpression of ARHGAP25 mutants on total and activated RAC content. *A) Representative images of total and active RAC and GAPDH content. B) Densitometric analysis of the* $log_2\frac{RAC}{GAPDH}$ *levels normalized. C) Densitometric analysis of the active RAC content. The* $log_2\frac{RAC_{GTP}}{RAC_{total}}$ *values were normalized to the vector. The box plot shows the median with the interquartile boxes and the corresponding min-to-max range (whiskers) of four independent measurements. Statistical analyses resulted in no significant results. Active RAC levels varied greatly between measurements. The figure contains new evaluations of our own published data (46).*

4.3. The effect of ARHGAP25 Ser-to-Ala mutants on F-actin levels

We examined the quantity of filamentous actin in the differentiated PLB-985 cells. Introduction of the S379-380A mutations was significantly highlighted as the main source of variation, based on the three-way ANOVA (24.1%; p=0.0014). When compared to the 'WT' group, the single mutants S363A and S488A exhibited functional similarities. Conversely, S379-380A and the double mutants increased the F-actin amount, although only the overexpression of the combined mutant S363A + S379-380A led to a significant difference compared to the 'WT' group (refer to Figure 9).

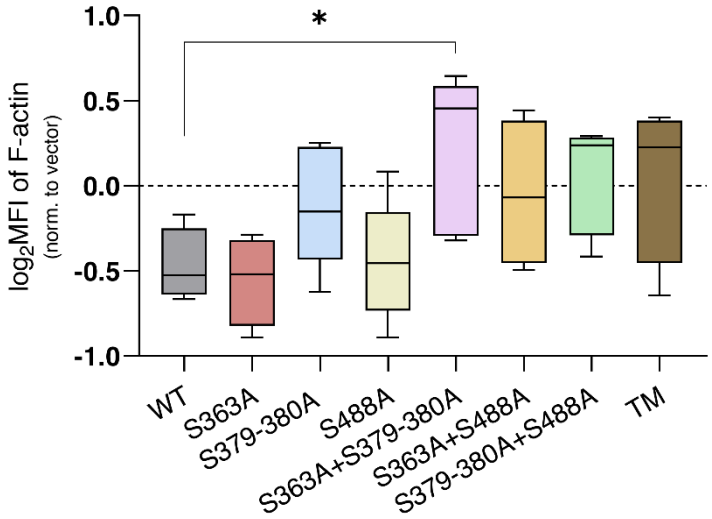

Figure 9. Evaluation of F-actin levels in transfected PLB-985 cells. *Cells were differentiated for 7 days, stained against F-actin, and measured with a flow cytometer. Logarithmized MFI values were normalized to the 'Vector', and phospho-mutants were compared to WT. The box plot shows the median with the interquartile (boxes) and the corresponding min-to-max range (whiskers) (n = 4–9). WT, S363A, and S488A samples showed decreased F-actin staining compared to the 'Vector'. Overexpression of the S363A-S379-380A mutant significantly elevated the F-actin levels. Statistics used: Three-way ANOVA followed by Dunnett's multiple comparisons test (compared to the 'WT' only): *: < 0.05. The figure is based on our own published data, but reprocessed and redesigned to fit the thesis (46).*

4.4. Evaluation of the neutrophil-specific pull-down with GST-fused ARHGAP25

GST and GST-tagged ARHGAP25 were incubated with intact neutrophil cell lysate, and the samples were analyzed using tandem mass spectrometry to identify the initial set of interaction partners. In the other six instances, the cell lysate was supplemented with nucleotide derivatives (GTPγS or GDPβS) to evaluate their impact on the detected protein pool. The label-free quantification intensity (LFQ) values were utilized to create a Principal Component Analysis (PCA) plot and a Pearson correlation matrix that served as quality control checks (Figure 10).

Distinct clusters were delineated on the PCA plot: the control samples, where the experiment was conducted with GST and intact cell lysates, were separate from the GST-ARHGAP25 pulldowns from the same lysates, as well as the pulldowns with GST-ARHGAP25 and the GTPγS- or GDPβS-modified lysates (Figure 10A). Similarly, pulldowns from identical protein pools (intact cell lysates, GDPβS-, and GTPγS-loaded cell lysates) exhibited a strong correlation with one another (Figure 10B). No clear indications of batch effect were observed.

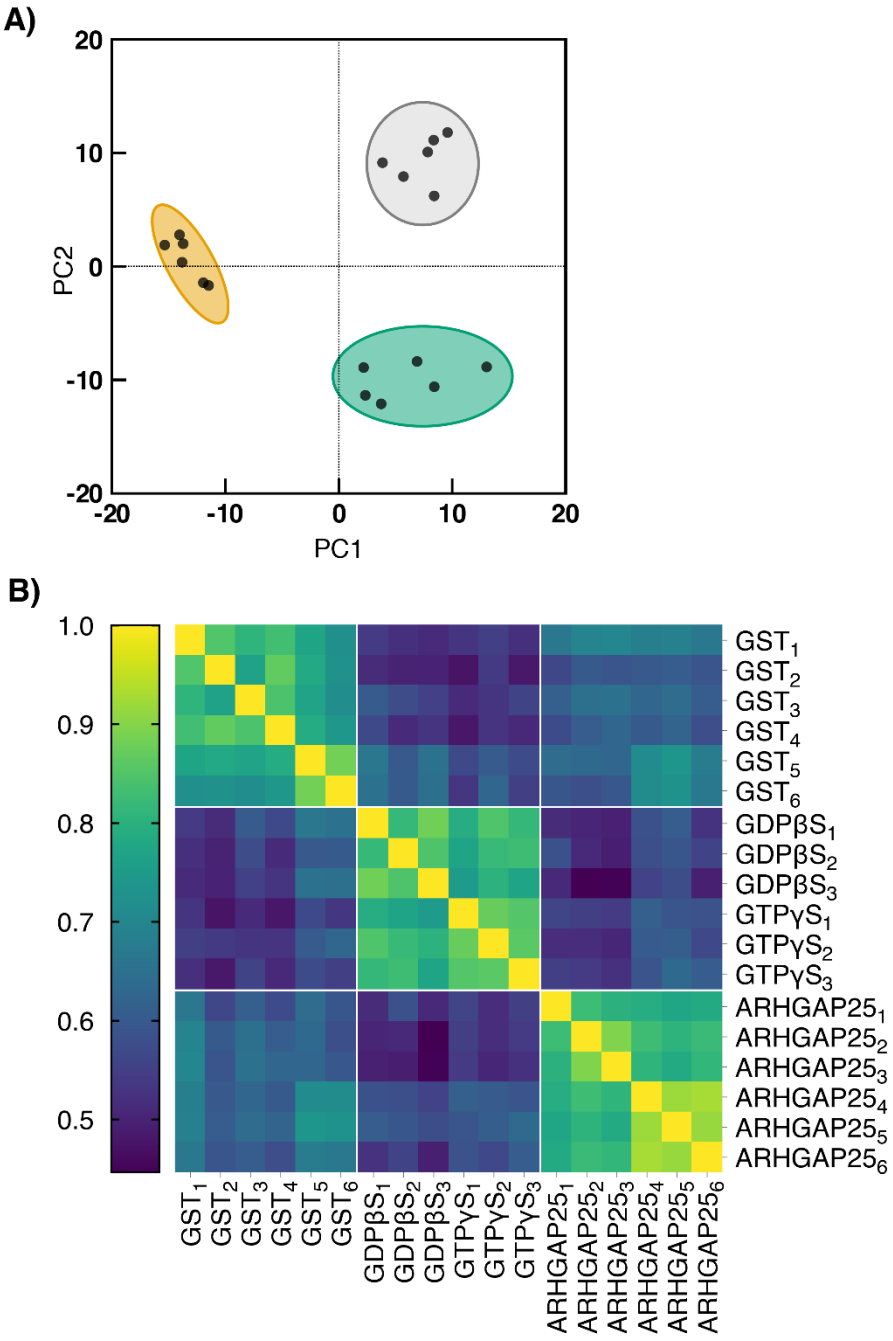

Figure 10. Quality control measurements before data analysis. *A) Principal component analysis (PCA) of the 'Label-Free Quantification' intensity (LFQ) values. The GST control + intact cell lysate (grey, n = 6), the GST-ARHGAP25 + intact cell lysate (green, n = 6), and the GST-ARHGAP25 + pretreated cell lysate (*yellow, *n = 3–3 with GDPβS and GTPγS, respectively) samples are clearly separate from one another. B) A heatmap showing the Pearson correlations calculated for each pair of samples, illustrating a similar segregation between the 3 groups. The figure is based on our own published data (86).*

The total amount of unique peptides and proteins identified in each sample before data imputation was assessed. GST-ARHGAP25 pulldowns consistently exhibited higher counts than GST control samples, indicating effective enrichment (Figure 11). Among the 775 identified proteins, 9.16% (71) were exclusively detected in GST, 60.77% (471) solely in GST-ARHGAP25 eluates, while 30.07% (233) were common to both. These findings imply that our recombinant GST-ARHGAP25 protein established direct or indirect interactions with multiple proteins.

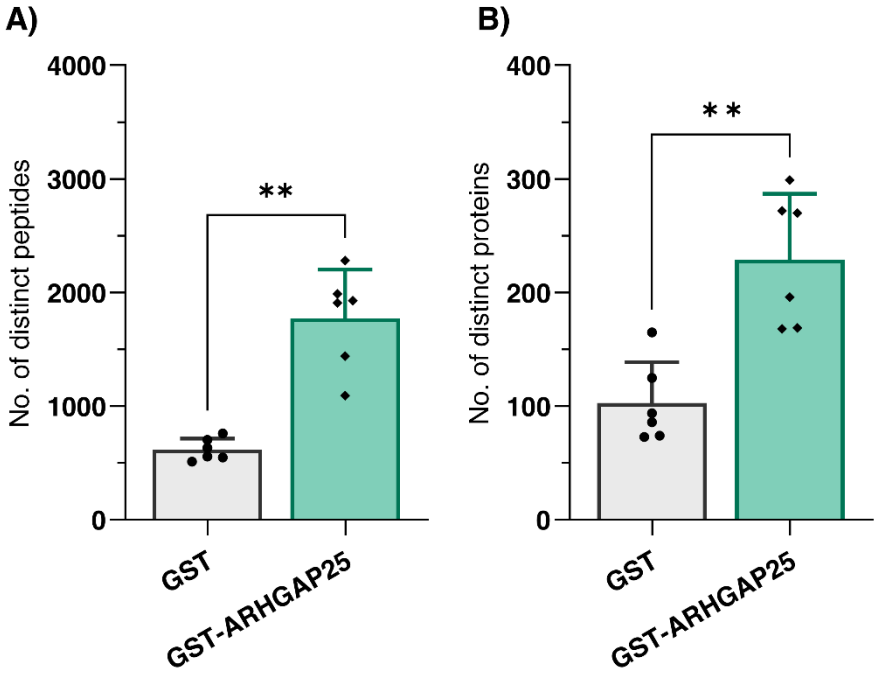

Figure 11. Enrichment of eluted proteins in the GST-ARHGAP25 samples. *The number of distinct peptides (A) and proteins (B) detected in GST-ARHGAP25 and GST samples (eluted from intact cell lysates) were compared. Eluted samples of GST-ARHGAP25 pull-downs consistently produced higher numbers. Applied statistics: unpaired T-test (**: $p < 0.01$). The figure is based on our own published data (86).*

4.5. Assessment of label-free quantitative proteomics to identify the ARHGAP25 proteome

For the creation of the initial interactome pool, we compared the GST-ARHGAP25 pulldown samples (eluted from intact neutrophil lysates) with the control GST pulldowns (eluted from the same lysates). Following statistical analysis utilizing multiple t-tests with

Benjamini–Hochberg correction, 90 proteins were identified as enriched in GST-ARHGAP25 eluates (Figure 12A; highlighted in green).

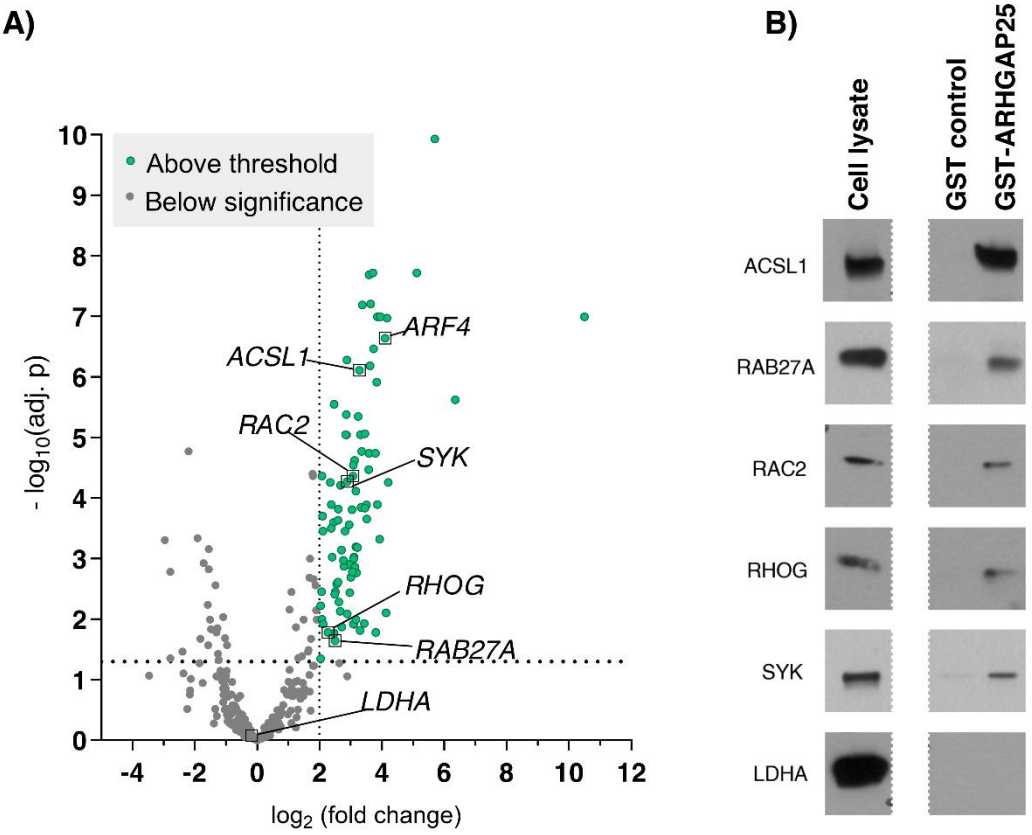

Figure 12. Identification of significantly enriched proteins. *A) A volcano plot was generated using logarithmized LFQ values of GTS-ARHGAP25 and GST control samples. Multiple t-tests with Benjamini–Hochberg correction were applied to determine the list of significantly enriched proteins. The significance threshold was set to log_2(fold change) = 2 and adj. p = 0.05. Significantly enriched proteins are colored green. B) Representative image created to illustrate the enrichment of different proteins detected by MS. Significantly enriched proteins (ACSL1, RAB27A, RAC2, RHOG, SYK) were identified by the respective antibodies, while LDHA, a protein that was not enriched in the GST-ARHGAP25 pull-down samples, was not detectable in the eluates. The figure is based on our own published data (86).*

The reliability of the MS data was assessed using six proteins chosen from the pulldown measurements. ACSL1, RAB27A, RAC2, RHOG, and SYK were picked from the significant candidates (upper right quadrant in Figure 12A), whereas LDHA was chosen from the proteins exhibiting low fold change and high adjusted p-value (bottom left). Figure 12B displays representative Western blots. All the chosen proteins were consistently identified by antibodies and exhibited substantial enrichment, except for LDHA, which was not detected by mass spectrometry either.

4.6. Refinement of the interactome by co-immunoprecipitation

In parallel, co-immunoprecipitation was performed using polyclonal anti-ARHGAP25 antibody and control IgG antibody, and the relative abundances of the previously identified 90 proteins were quantified via mass spectrometry. Each candidate was given a confidence level ('high,' 'moderate,' or 'unlikely') determined by the protein detection rate and an enrichment score ('high' or 'low') based on the fold change values determined by co-immunoprecipitation. Among the 90 previously identified candidates, 13 were eliminated because of insufficient detection rates, whereas the results validated the enrichment of 76 proteins (excluding ARHGAP25). The potential interactions were classified into three categories based on their designated confidence and enrichment scores:

- 16 interactions were deemed ‘low credibility’ (indicating moderate confidence and low enrichment),
- 26 were rated ‘satisfactory’ (exhibiting either high confidence with low enrichment or moderate confidence with high enrichment),
- and 34 were assigned a ‘high credibility’ rating (characterized by high confidence and enrichment).

To explore the known interactions among these candidates, we employed the STRING (Search Tool for Retrieval of Interacting Genes/Proteins) platform to compile all experimentally validated interactions. This yielded a total of 49 connections involving 45 interactors, suggesting the potential presence of eluted multimers in the samples.

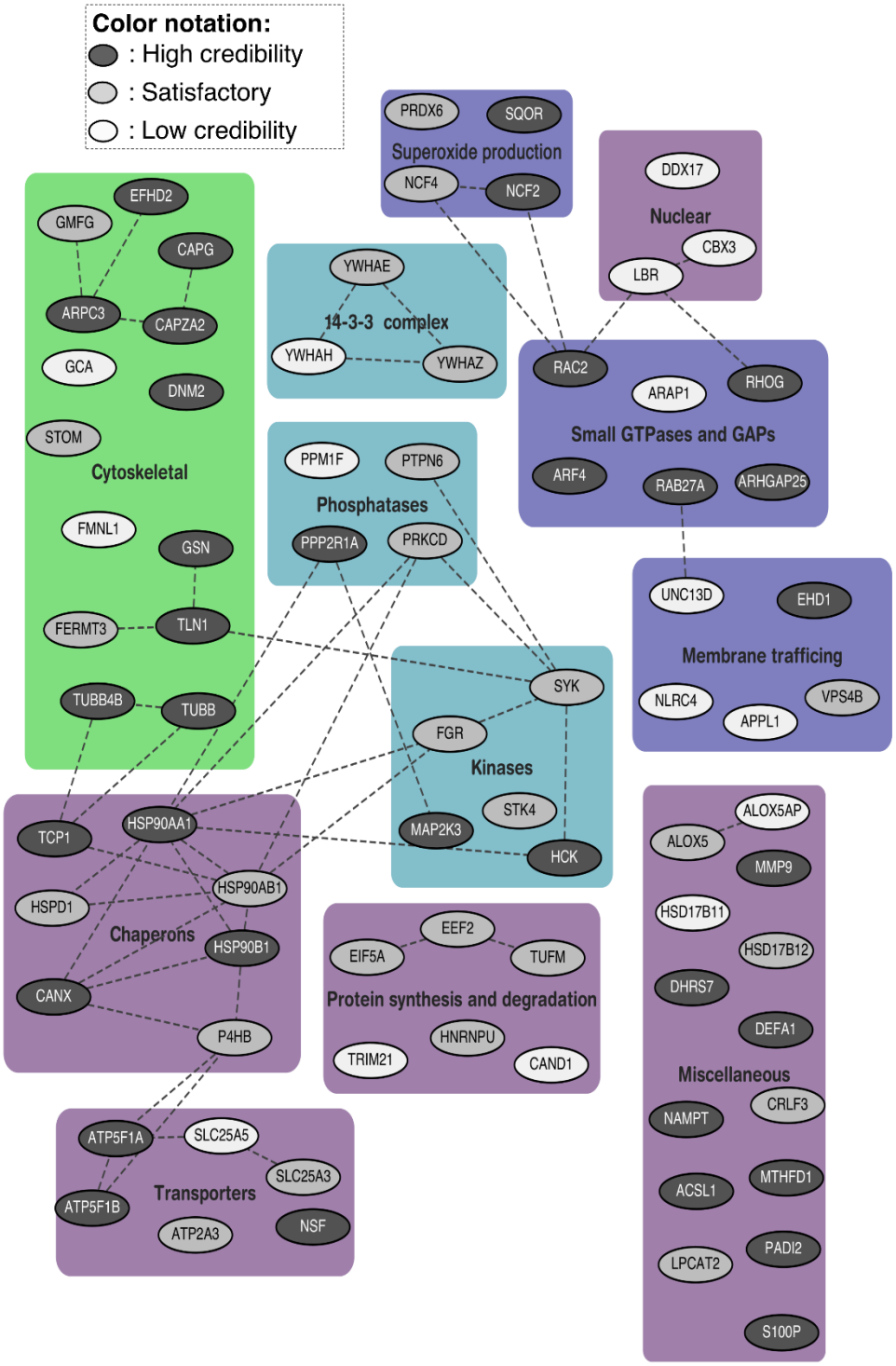

Figure 13. Visualization of the neutrophil-specific interactome of ARHGAP25. *All candidates were manually categorized based on cellular localization or function. The dashed lines denote known physical interactions extracted from the STRING database. The likelihood of the association with ARHGAP25 is presented by the color of the nodes: dark grey, medium grey, and light grey, referring to high credibility, satisfactory, and low credibility, respectively. The figure is based on our own published data (86).*

Next, the candidates were categorized based on subcellular localization and molecular function to create a visual representation of the identified proteome in a visually digestible form (Figure 13). In addition to the anticipated presence of cytoskeletal and GTPase-related proteins, several kinases, phosphatases, and chaperones were found. Members of the 14-3-3 family were also present, along with proteins associated with membrane trafficking, protein synthesis, and degradation.

4.7. Investigation of biological functions of the revealed proteome

Considering the presence of numerous associations, we sought to understand whether the identified set of proteins was connected to similar intracellular functions or pathways. Functional enrichment analysis was performed utilizing the ShinyGO web server. Compared to the neutrophil proteome, our results indicated over-represented gene sets that predominantly grouped into 10 principal themes (refer to Figure 14). First, we identified a cluster of five gene sets connected with the Fc receptor signaling pathway and phagocytosis. The corresponding proteins were also represented in interleukin-mediated signaling and phosphorylation. Several terms that involve cell projection and cytoskeletal organization emerged, with some tied to GTPase-mediated signaling. Additionally, gene sets associated with mast cell and platelet activation, hemostasis, and organelle maintenance were over-represented as well.

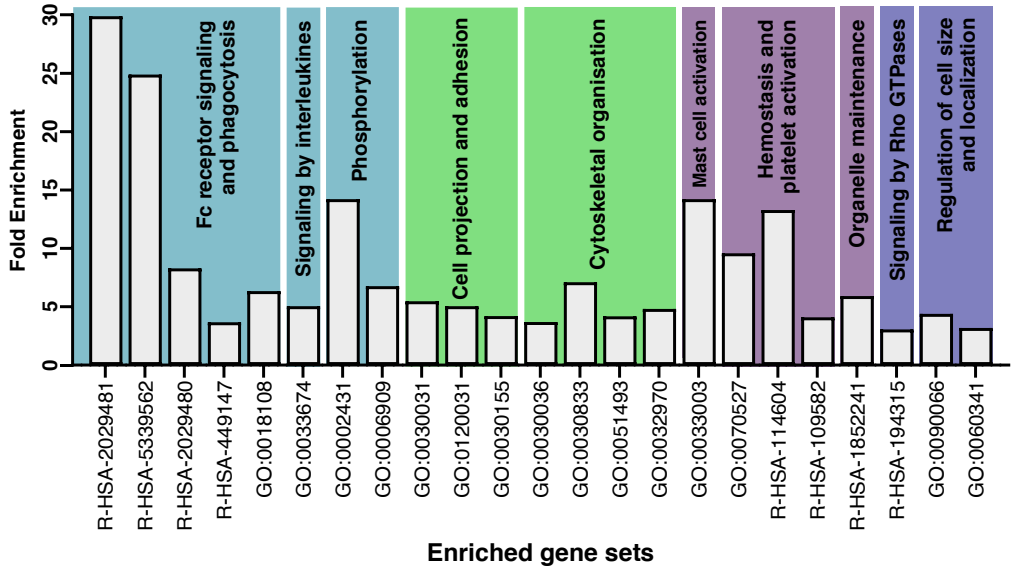

Figure 14. Functional analysis of the identified candidates. *Functional enrichment analysis was carried out on the identified candidates as described in the 'Methods' section. The enriched gene sets were grouped based on similarities in the biological functions: Fc receptor-mediated signaling and phagocytosis-related functions and phosphorylation-related terms (colored light blue); cytoskeletal remodeling, cell projections, and adhesion (colored green); mast cell activation, hemostasis, platelet activation, and organelle maintenance (colored purple); and Rho-GTPases and their signaling-related terms (colored dark blue). The figure is based on our own published data (86).*

4.8. Investigation of the effects of GTPγS or GDBβS loading of small GTPases on the proteome

Among the 76 proteins, four small GTPases were identified in the GST-ARHGAP25 eluates. RAC2, a member of the Rac subclass mostly found in neutrophilic granulocytes, demonstrated an average fold change of 3.08 and 2.57 in the pulldown and co-immunoprecipitation tests, respectively. Notably, another member of the Rac subfamily, RHOG, was identified in 4 pulldowns (67%) and all co-immunoprecipitation samples, demonstrating a fold change of 2.28 and 2.75 in the pulldown and co-IP analyses, respectively. Consistent with prior findings, we found no evidence that any members of the Rho or Cdc42 subclasses eluted with GST-ARHGAP25. Unexpectedly, ARF4 and RAB27A were identified as possible protein interactions as well.

To explore the influence of GTP/GDP on the previously identified interactions, we performed GTPγS and GDPβS loading of the cell lysate prior to incubation with the beads. These GTP- and GDP-analogues can bind to the same pocket as their endogenous counterparts, but cannot be hydrolyzed or detached (93, 94). During the loading process, the ratio of active (GTPγS-bound) to inactive (GDPβS-bound) states is altered to favor one state, enabling us to examine the impact of the GTP/GDP cycle on the interactome. Upon analyzing the four designated small G-proteins separately, we observed distinct LFQ values following GTPγS loading in contrast to GDPβS for RAC2 ($log_2FC = 0.785$) and RHOG ($log_2FC = 0.589$). Conversely, ARF4 and RAB27A exhibited little variation ($log_2FC < 0.2$) (Figure 15A). Western blot assays further corroborated the prior findings on RAC2 and RHOG (Figure 15B). The data may indicate ARHGAP25's affinity for the active (GTP-bound) forms of RAC2 and RHOG, consistent with the GAP domain's recognized specificity for the Rho family. Nonetheless, the binding appears to be independent of the GDP/GTP-bound state concerning ARF4 and RAB27A.

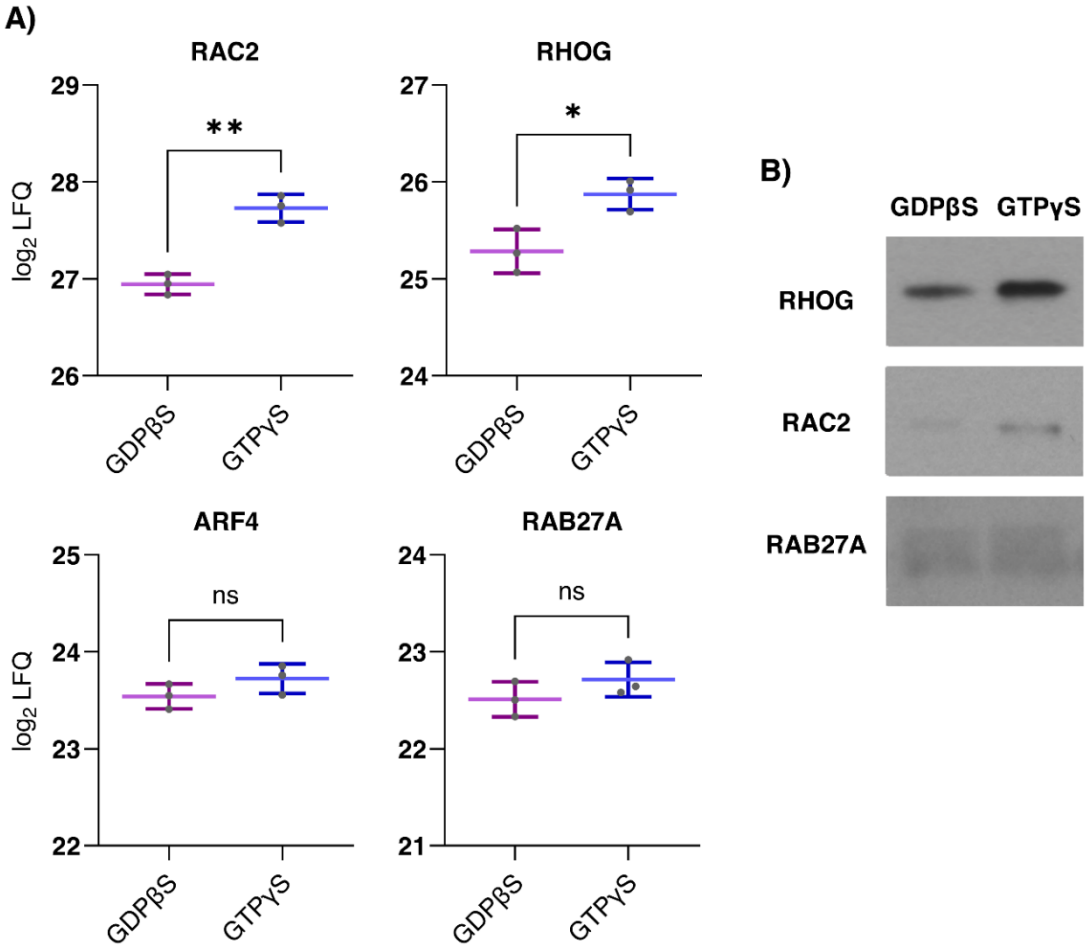

Figure 15. Effect of GTPγS- or GDPβS-loading on the ARGAP25-GTPase interactions. *Pulldowns carried out from GTPγS- or GDPβS-loaded samples were used to shift the state of GTPases towards the active or inactive form prior to pulldowns with ARHGAP25-GST. A) The change in LFQ values related to the detected GTPases was assessed. RAC2- and RHOG-related LFQ values were significantly elevated in GTPγS-loaded pull-downs, while ARF4 and RAB27A were not. B) Representative Western blot images of the eluate. Applied statistics: unpaired T-test (ns: ≥0.05; *: < 0.05; **: < 0.01). The figure is based on our own published data (86).*

4.9. In silico investigation of the RHOG-ARHGAP25 dimer

Given the large number of identified candidates and the overrepresentation of existing interactions among them, we attempted to highlight the proteins that are the most likely direct partners for ARHGAP25. We utilized AlphaFold Multimer prediction to ascertain reliable direct binary interactions between ARHGAP25 and the candidates. We selected 28 identified proteins for simulating protein-complex formation based on fold change values, intracellular localization, and protein function. For each dimer, ten predictions were executed, and the predictions were compared based on the estimates established by the creators of Alphafold: the TM-score (pTM) and intracellular TM-score (ipTM), derived from a pairwise error prediction computed as a linear projection from the final pair representation (72, 91). In accordance with the directives of O'Reilly et al., all predictions with ipTM < 0.55 were disregarded, and a threshold of ipTM = 0.85 was chosen to identify the most reliable predictions (see Figure 16A).(95) The software generated three dimers involving ARHGAP25 and RAC2, RHOG, and RAB27A above the initial cut-off value. Given that only the predictions for RHOG and RAC2 had the highest credibility (exceeding 0.85 ipTM), we only focused on their predicted conformation in this study. Upon closer inspection of the predicted models, both small GTPases were situated next to the GAP domain of ARHGAP25 (Figure 16B and C, highlighted in green), exhibiting the lowest predicted alignment errors in that region. The predicted aligned error plots assess the anticipated positional error for each residue in a predicted protein structure (72). Thus, the relative position of the corresponding protein segments at the simulated interaction site (namely, the GAP domain and the majority of the small GTPase) is considered accurate. Based on the simulations, the GAP domain predominantly participates in the interaction, whereas the PH domain and the coiled-coil region contribute to a lesser extent.

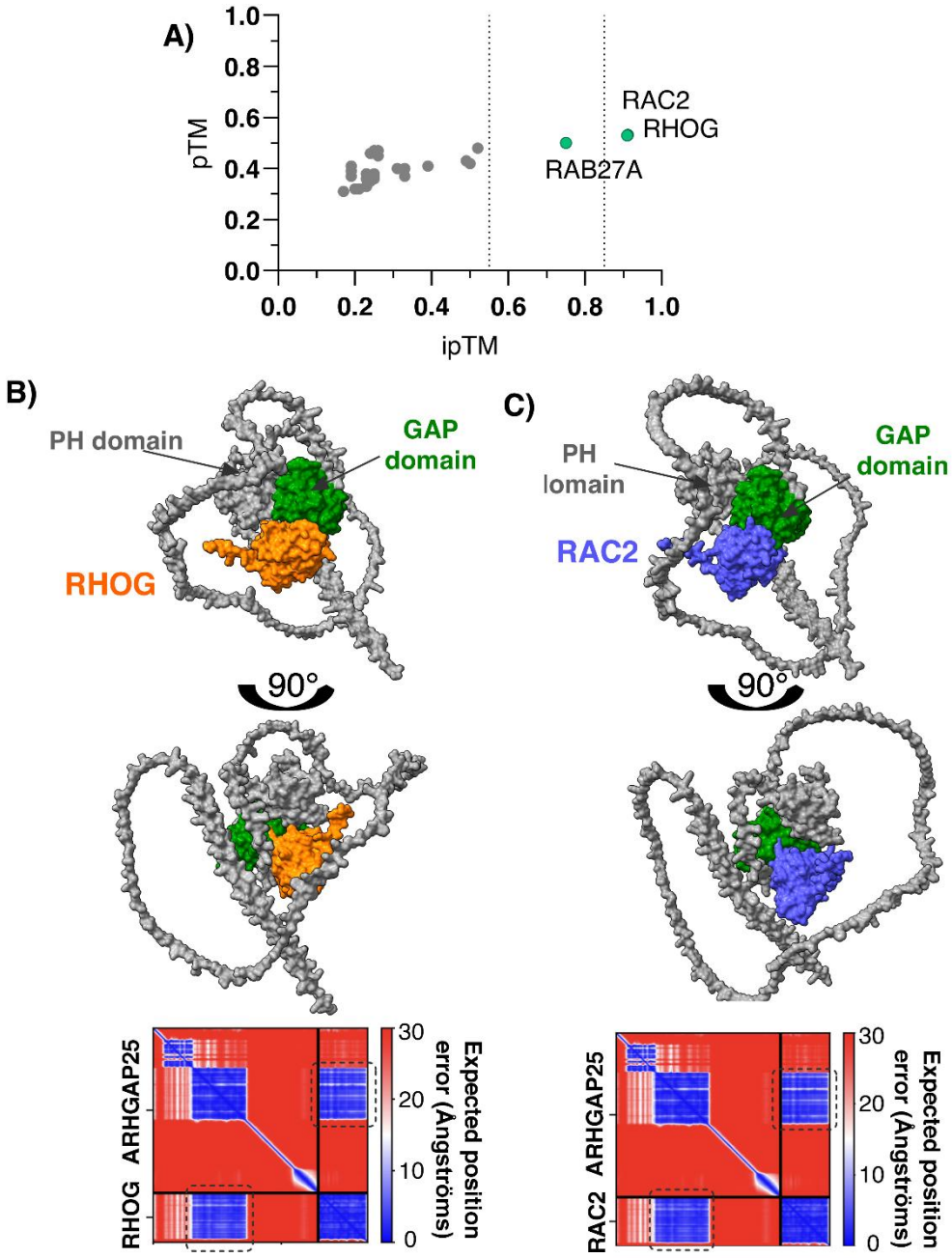

Figure 16. In silico prediction of the ARHGAP25-RAC2 and the ARHGAP25-RHOG complexes. *A) Evaluation of dimer simulation results between candidates and ARHGAP25. The credibility of the dimers was assessed by their pTM and ipTM values. ARHGAP25-RAC2 and ARHGAP25-RHOG provided predictions with the highest ipTM values and were chosen for further assessment. B) 3D model of the RHOG (orange) and the ARHGAP25 (grey, but the GAP domain is highlighted in green) complex. C) 3D representation of the RAC2 (blue) and the ARHGAP25 (grey, but the GAP domain is highlighted in green) complex. The corresponding PAE plots are presented in C and D. The figure is based on our own published data (86).*

4.10. Demonstration of the phosphorylation-dependent interaction between 14-3-3 proteins and ARHGAP25

Given that three members of the 14-3-3 proteins were identified as potential interaction partners, we aimed to evaluate the likelihood of their binding to ARHGAP25 by in silico prediction. The 14-3-3-Pred web server, developed by Madeira et al., utilizes three distinct methodologies—position-specific scoring matrix, support vector machines (SVM), and artificial neural network (ANN) classification—to predict potential residues for 14-3-3 binding following phosphorylation. When running the prediction with ARHGAP25's sequence ('Isoform 1'), T102, S395, S500, and T502 achieved high scores by a single approach, while S25, T343, T442, and S487 received high scores across all three methods. The actual scores are available as supplement material online (86). The detected phosphosites are depicted in Figure 17A.

To see whether phosphorylation facilitates the interaction, we performed pulldowns with and without prior phosphorylation on ARHGAP25. The amount of the eluted 14-3-3 proteins was visualized by an anti-pan 14-3-3 antibody. Only pre-phosphorylated GST-ARHGAP25 associated with a detectable amount of 14-3-3 proteins (Figure 17B).

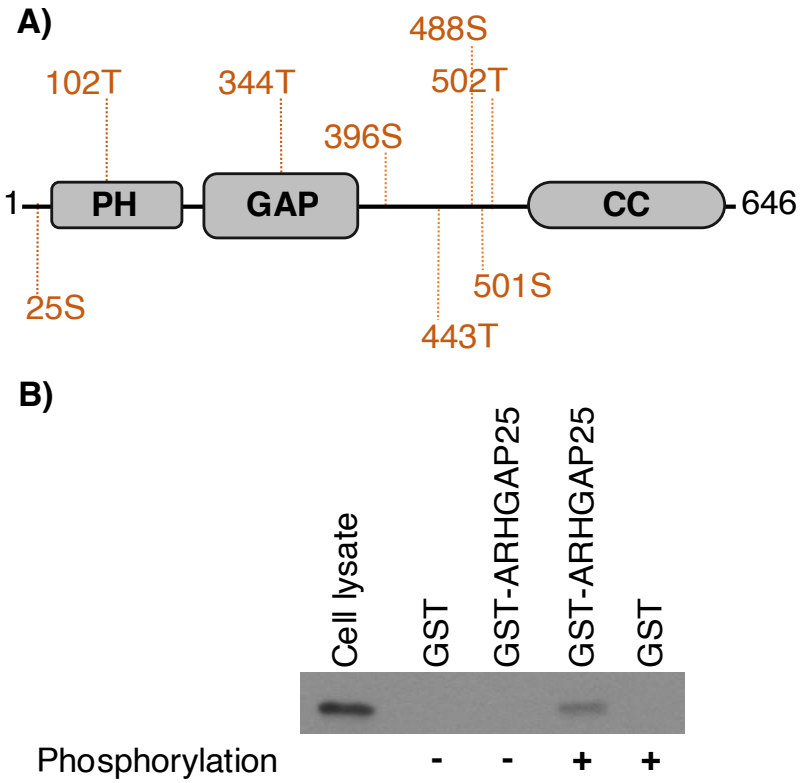

Figure 17. Phosphorylation-dependent interaction between 14-3-3 and ARHGAP25. *A) Graphical representation of the full-length ARHGAP25 (isoform 4) along with the potential binding sites for 14-3-3 proteins (in orange) identified in silico. PH (pleckstrin homology) domain, GAP domain, CC (coiled-coil) region. B) Phosphorylation-dependent interaction between GST-ARHGAP25 and 14-3-3 proteins. Pulldown was performed with and without prior phosphorylation of the bait. 14-3-3 proteins were detectable with the anti-pan 14-3-3 antibody (cat. no: 8312; Cell Signaling Technology®) after Western blot only in samples using phosphorylated GST-ARHGAP25. The blot is representative of 2 experiments. The figure is based on our own published (A) and unpublished (B) data (86).*

5. Discussion

Several studies over the past decade have examined the involvement of ARHGAP25 in immunological processes through *in vitro* and cell-based techniques, as well as in animal models, demonstrating the diverse functions of a protein with a singular known enzymatic activity. From the very beginning, data indicated that ARHGAP25 is subject to regulation, as its protein and mRNA levels decline upon particular stimuli (8), but the reasons are still unknown. Wang *et al.*, in collaboration with our research group, were the first to report that the phosphorylation of ARHGAP25 might affect HSPC migration (41). Subsequently, our group demonstrated that the phosphorylation of ARHGAP25 reduces its GAP activity *in vitro*, an effect that was mitigated in the S363A and S488A but not in the S379-380A single mutant (46).

To further investigate how phosphorylation can influence ARHGAP25, we overexpressed the previously mentioned Ser-to-Ala mutants in PLB-985 cells, a human cell line that can be differentiated into neutrophil-like cells. Upon confirming the success of the transfections, we assessed the total and activated RAC levels in the cells, given ARHGAP25's connection to RAC. In contrast to the in vitro results, the introduction of the S379-380A mutation was the source of the biggest variation in the measured RAC levels, albeit failing to reach statistical significance. All PLB-985 cells with mutation-bearing ARHGAP25 showed an elevation in RAC content to a certain degree, but none of the differences were statistically significant compared to the 'WT' group. The PAK-PBD-mediated RAC-GTP-pulldown experiments showed great variability among the independent measurements, with no clear pattern identified. Even though the RAC-related measurements did not provide clear insight, the filamentous actin levels appeared to be affected differently among the phospho-mutants. WT, S363A, and S488A-overexpressing cells exhibited equally lower F-actin levels compared to the 'Vector,' while this decrease was not present in the S379-380A, the double, and the triple mutant-expressing cells. Three-way ANOVA highlighted the S379-380A mutation as the significant source of the biggest variation, coinciding with the previously mentioned results regarding the RAC levels, as well as other published results regarding phagocytosis and superoxide production (46). We hypothesize that the serine residues at the 379th and 380th positions might play a key role in ARHGAP25's ability to regulate

actin depolymerization, a process that is a spatially critical event during phagocytosis and requires multiple additional proteins besides RAC.

Our objective was to compile a list of protein partners utilizing human neutrophilic granulocytes as the pool. This could provide an environment for our bait to form associations pertinent to its intracellular behavior. We combined GST-tagged pulldowns and co-immunoprecipitation using endogenous ARHGAP25, as their advantages and setbacks complement each other. The initial GST pulldowns were deemed successful and generated an initial list of 90 partners. The reliability of these results was corroborated by Western blot studies, which confirmed the presence of some detected proteins in the MS report. Next, we compared these results with co-immunoprecipitations using polyclonal antibodies against ARHGAP25 and excluded the candidates that had not been detected in those samples. The remaining 76 proteins were further categorized based on the enrichment and detection rates to offer an estimation of our candidates' credibility. Despite the sizable list of candidates, the overlap with datasets listed in Tables 1 and 2 is minimal: only PPP2R1A can be found in both. Even though this was anticipated based on our concerns, it is vital to examine the candidates in more detail to assess the plausibility of our findings. Nonetheless, our list provides a more plausible interaction profile for ARHGAP25, especially when we compare these results to the processes ARHGAP25 participates in. Unlike in the existing databases, two components of the soluble part of the NADPH oxidase complex (NCF2 and NCF4) appeared in our results, which was anticipated based on ARHGAP25's known role in RAC-mediated superoxide generation in neutrophils (38). Moreover, numerous novel promising candidates (*e.g.*, proteins associated with membrane trafficking, transporters, and the ARP2/3 complex) emerged from our experiment, which could serve as the foundation for future projects.

Several small G proteins emerged from our identified candidates, including RAC2. Human neutrophils express two isoforms of RAC (RAC1 and RAC2), with a predominance of RAC2 (96, 97). Even though previous *in vitro* studies defined ARHGAP25 specificity to RAC1 (33), this is the first report of the RAC2-ARHGAP25 interaction. Four identified peptide sequences were exclusive to RAC2, while we did not identify any RAC1-specific unique peptides by mass spectrometry (data not shown in this thesis but available in the published supplementary material) (86). Nonetheless, considering the elevated RAC2 levels in neutrophils and the 92% homology between the

two proteins, the absence of RAC1-specific peptides does not exclude the possibility of an interaction with ARHGAP25. As an unexpected candidate, RHOG, another member of the Rac subfamily, was identified and corroborated by co-immunoprecipitation, along with ARF4 and RAB27A. Despite their unexpected appearance, Müller *et al.* also found evidence of an interaction between ARHGAP31 and ARF4 during their experiments (78). Kouchi *et al.* documented analogous findings between ARHGAP21, ARHGAP23, and Arf members (98). Via computational analyses, they identified the PH domain of the GAPs as candidate interaction locations. Our data suggest that the substrate specificity of ARHGAP25 may be more varied than previously assumed. *In silico* prediction using the AlphaFold Multimer algorithm generated reliable dimers of ARHGAP25-RAC2 and ARHGAP25-RHOG. Upon closer inspection, the position of the two small GTPases was similar, being in close proximity to the GAP domain and moderately associated with the PH domain. This positioning could enable the GTP-hydrolysis during interaction. During the GTP–GDP cycle of small GTPases, the active form favors binding to GAPs over GEFs, prompting us to examine the effect of GTP/GDP binding on the interaction with ARHGAP25 (76). Our MS and Western blot results indicate that ARHGAP25 exhibits a preference for the GTPγS-bound forms of RAC2 and RHOG over their inactive GDBβS-bound states. However, no such preference was detected for ARF4 and RAB27A. We hypothesize that either ARHGAP25 may act as a GTPase-activating enzyme for RAC2 and RHOG, or it may participate in a molecular complex including active RAC2 and RHOG. Nevertheless, our results indicate just a physical association among these proteins, necessitating more investigations to assess the GAP activity of ARHGAP25 on these small GTPases as well.

It has been established that ARHGAP25 can be phosphorylated and potentially dephosphorylated in neutrophils during intracellular events (46). Even though the existing PPI databases list possible kinases for ARHGAP25, we wanted to revisit this question with a cell-specific approach. The study presented five kinases (HCK, FGR, MAP2K3, STK4, and SYK) and four phosphatases (PRKCD, PPM1F, PPP2R1A, and PTPN6) as potential interacting partners, and the related interleukin- and Fc-receptor-mediated pathways. As SYK-mediated RAC activation by GEFs (99) has already been reported, regulation of ARHGAP25's effect on RAC inhibition by these upstream regulators could

present a plausible complementary means for Fc receptor-mediated RAC activation. Nevertheless, more studies are required to validate this correlation at the cellular level.

YWHAE, YWHAZ, and YWHAH, members of the 14-3-3 protein family, have also been highlighted, which are known for their diverse regulatory roles carried out via phosphorylation-dependent interactions (100, 101). This phenomenon has been investigated regarding SOS1, a RAS-specific guanine nucleotide exchange factor (102), but many other investigations on GAP PPIs identified members of the 14-3-3 family as potential candidates (78). Our in silico analysis identified eight phosphosites on ARHGAP25 as potential interaction sites, including S488. Moreover, we demonstrated that prior phosphorylation of GST-ARHGAP25 enables the association with 14-3-3 proteins. Although investigating the influence of 14-3–3 proteins on ARHGAP25 functions is beyond the scope of this dissertation, this interaction could be a potential new mechanism for ARHGAP25 regulation.

6. Conclusions

In this thesis, I sought to further our understanding of ARHGAP25 at a molecular level. We employed cell-based approaches to explore the potential involvement of ARHGAP25 phosphorylation in RAC and F-actin regulation, along with *in vitro* techniques to identify protein partners or regulators that may engage in ARHGAP25-mediated processes.

The following goals were achieved

I. We quantified and compared the total and activated RAC content in PLB-985 cell cultures overexpressing the Ser-to-Ala ARHGAP25 mutants. Even though the introduction of the mutations did not have a clear effect on RAC-GTP levels, the presence of the S379-380A mutation influenced ARHGAP25's effect on filamentous actin levels, dampening the F-actin-lowering effect of ARHGAP25 overexpression.

II. We established a neutrophil-specific interactome combining GST-pulldown and co-immunoprecipitation techniques, resulting in 76 identified partners that complement ARHGAP25's known profile, as well as highlighting new directions for ARHGAP25-related research.

III. Apart from the most anticipated, but still novel RAC2-ARHGAP25 interaction, we identified three other small GTPases (RHOG, ARF4, RAB27A) as potential interaction partners. We showed via in silico simulations that ARHGAP25's associations with RHOG and RAC2 were GAP-domain related, and in vitro manipulation of the small GTPases' activity influenced the interactions in a similar fashion. We identified a promising new list of kinases and phosphatases, mainly related to the Fc-receptor and interleukin-mediated signaling, and we confirmed a novel phosphorylation-dependent interaction between ARHGAP25 and 14-3-3 protein family members, serving as promising new directions for the research related to ARHGAP25 regulation.

7. Summary

ARHGAP25 is a GTPase-activating protein playing a regulatory role in neutrophils and potentially other leukocytes. Nonetheless, many details remain unresolved, particularly regarding its intracellular behavior. This thesis aims to expand our current knowledge and uncover unexplored areas related to this protein.

First, we examined its phosphorylation-dependent functions in vivo by generating and transfecting overexpressed Ser-to-Ala mutants in PLB-985 cells and measuring their RAC levels, along with their F-actin content. The overexpression of the mutation-bearing ARHGAP25 proteins did not have a clear effect on RAC-activation, but the S379+380 phosphosites were deemed relevant for the regulation of filamentous actin levels.

To pinpoint protein interactions and pathways involved with ARHGAP25, we compiled a list of protein partners using human neutrophilic granulocytes as the starting material, yielding 76 proteins. Subsequent functional enrichment analysis identified several expected and novel cellular functions based on the list, proposing new perspectives to ARHGAP25-related research.

The results identified 14-3-3 members as candidates. In silico analysis identified eight potential interaction sites on ARHGAP25, and we demonstrated that prior phosphorylation of GST-ARHGAP25 facilitates its association with 14-3-3 proteins. This interaction may represent a novel mechanism for the regulation of ARHGAP25, though additional research is required to support this hypothesis.

The identification of four small G proteins (RAC2, RHOG, ARF4, and RAB27A) produced novel results. The following *in silico* studies corroborated the viability of the interaction between RHOG and ARHGAP25, associated via ARHGAP25's GAP domain, and the interaction was influenced by the activation cycle of the small GTPase.

8. References

1. (2025) NobelPrize.org., p. All Nobel Prizes in Physiology or Medicine.
2. Zhang M, Chen T, Lu X, Lan X, Chen Z, Lu S. (2024) G protein-coupled receptors (GPCRs): advances in structures, mechanisms, and drug discovery. Signal Transduct Target Ther, 9: 88.
3. Goitre L, Trapani E, Trabalzini L, Retta SF. (2014) The Ras superfamily of small GTPases: the unlocked secrets. Methods Mol Biol, 1120: 1–18.
4. Yin G, Huang J, Petela J, Jiang H, Zhang Y, Gong S, Wu J, Liu B, Shi J, Gao Y. (2023) Targeting small GTPases: emerging grasps on previously untamable targets, pioneered by KRAS. Signal Transduct Target Ther, 8: 212.
5. Pai EF, Kabsch W, Krengel U, Holmes KC, John J, Wittinghofer A. (1989) Structure of the guanine-nucleotide-binding domain of the Ha-ras oncogene product p21 in the triphosphate conformation. Nature, 341: 209–214.
6. Traut TW. (1994) Physiological concentrations of purines and pyrimidines. Mol Cell Biochem, 140: 1–22.
7. Cromm PM, Spiegel J, Grossmann TN, Waldmann H. (2015) Direct Modulation of Small GTPase Activity and Function. Angew Chem Int Ed Engl, 54: 13516–13537.
8. Csépányi-Kömi R, Pásztor M, Bartos B, Ligeti E. (2018) The neglected terminators: Rho family GAPs in neutrophils. European Journal of Clinical Investigation, 48.
9. Bos JL, Rehmann H, Wittinghofer A. (2007) GEFs and GAPs: critical elements in the control of small G proteins. Cell, 129: 865–877.
10. DerMardirossian C, Bokoch GM. (2005) GDIs: central regulatory molecules in Rho GTPase activation. Trends Cell Biol, 15: 356–363.
11. Faulkner B, He Y, Sitrin D, Stains CI. (2025) Methods for Controlling Small GTPase Activity. Chembiochem, doi:10.1002/cbic.202500156: e2500156.
12. Wennerberg K, Rossman KL, Der CJ. (2005) The Ras superfamily at a glance. J Cell Sci, 118: 843–846.
13. Simanshu DK, Nissley DV, McCormick F. (2017) RAS Proteins and Their Regulators in Human Disease. Cell, 170: 17–33.

14. Rojas AM, Fuentes G, Rausell A, Valencia A. (2012) The Ras protein superfamily: evolutionary tree and role of conserved amino acids. J Cell Biol, 196: 189–201.
15. Madaule P, Axel R. (1985) A novel ras-related gene family. Cell, 41: 31–40.
16. Bar-Sagi D, Hall A. (2000) Ras and Rho GTPases: a family reunion. Cell, 103: 227–238.
17. Haga RB, Ridley AJ. (2016) Rho GTPases: Regulation and roles in cancer cell biology. Small GTPases, 7: 207–221.
18. Tybulewicz VL, Henderson RB. (2009) Rho family GTPases and their regulators in lymphocytes. Nat Rev Immunol, 9: 630–644.
19. Verboon JM, Parkhurst SM. (2015) Rho family GTPases bring a familiar ring to cell wound repair. Small GTPases, 6: 1–7.
20. Mosaddeghzadeh N, Ahmadian MR. (2021) The RHO Family GTPases: Mechanisms of Regulation and Signaling. Cells, 10.
21. Lawson CD, Ridley AJ. (2018) Rho GTPase signaling complexes in cell migration and invasion. J Cell Biol, 217: 447–457.
22. Csepanyi-Komi R, Levay M, Ligeti E. (2012) Rho/RacGAPs: embarras de richesse? Small GTPases, 3: 178–182.
23. Symons M, Settleman J. (2000) Rho family GTPases: more than simple switches. Trends Cell Biol, 10: 415–419.
24. Aspenstrom P. (2020) Fast-cycling Rho GTPases. Small GTPases, 11: 248–255.
25. Aspenstrom P, Ruusala A, Pacholsky D. (2007) Taking Rho GTPases to the next level: the cellular functions of atypical Rho GTPases. Exp Cell Res, 313: 3673–3679.
26. Shutes A, Berzat AC, Cox AD, Der CJ. (2004) Atypical mechanism of regulation of the Wrch-1 Rho family small GTPase. Curr Biol, 14: 2052–2056.
27. Troeger A, Chae HD, Senturk M, Wood J, Williams DA. (2013) A unique carboxyl-terminal insert domain in the hematopoietic-specific, GTPase-deficient Rho GTPase RhoH regulates post-translational processing. J Biol Chem, 288: 36451–36462.
28. Aspenstrom P, Fransson A, Saras J. (2004) Rho GTPases have diverse effects on the organization of the actin filament system. Biochem J, 377: 327–337.

29. Berthold J, Schenkova K, Ramos S, Miura Y, Furukawa M, Aspenstrom P, Rivero F. (2008) Characterization of RhoBTB-dependent Cul3 ubiquitin ligase complexes--evidence for an autoregulatory mechanism. Exp Cell Res, 314: 3453–3465.
30. Wilkins A, Carpenter CL. (2008) Regulation of RhoBTB2 by the Cul3 ubiquitin ligase complex. Methods Enzymol, 439: 103–109.
31. Wilkins A, Ping Q, Carpenter CL. (2004) RhoBTB2 is a substrate of the mammalian Cul3 ubiquitin ligase complex. Genes Dev, 18: 856–861.
32. Katoh M, Katoh M. (2004) Identification and characterization of ARHGAP24 and ARHGAP25 genes in silico. Int J Mol Med, 14: 333–338.
33. Csépányi-Kömi R, Sirokmány G, Geiszt M, Ligeti E. (2012) ARHGAP25, a novel Rac GTPase-activating protein, regulates phagocytosis in human neutrophilic granulocytes. Blood, 119: 573–582.
34. Makitie RE, Henning P, Jiu Y, Kampe A, Kogan K, Costantini A, Valimaki VV, Medina-Gomez C, Pekkinen M, Salusky IB, Schalin-Jantti C, Haanpaa MK, Rivadeneira F, Bassett JHD, Williams GR, Lerner UH, Pereira RC, Lappalainen P, Makitie O. (2021) An ARHGAP25 variant links aberrant Rac1 function to early-onset skeletal fragility. JBMR Plus, 5: e10509.
35. Uhlén M, Björling E, Agaton C, Szigyarto CA, Amini B, Andersen E, Andersson AC, Angelidou P, Asplund A, Asplund C, Berglund L, Bergström K, Brumer H, Cerjan D, Ekström M, Elobeid A, Eriksson C, Fagerberg L, Falk R, Fall J, Forsberg M, Björklund MG, Gumbel K, Halimi A, Hallin I, Hamsten C, Hansson M, Hedhammar M, Hercules G, Kampf C, Larsson K, Linskog M, Lodewyckx W, Lund J, Lundeberg J, Magnusson K, Malm E, Nilsson P, Ödling J, Oksvold P, Olsson I, Öster E, Ottosson J, Paavilainen L, Persson A, Rimini R, Rockberg J, Runeson M, Sivertsson Å, Sköllermo A, Steen J, Stenvall M, Sterky F, Strömberg S, Sundberg M, Tegel H, Tourle S, Wahlund E, Waldén A, Wan JH, Wernérus H, Westberg J, Wester K, Wrethagen U, Xu LL, Hober S, Pontén F. (2005) A human protein atlas for normal and cancer tissues based on antibody proteomics. Molecular & Cellular Proteomics, 4: 1920–1932.
36. Uhlen M, Fagerberg L, Hallström BM, Lindskog C, Oksvold P, Mardinoglu A, Sivertsson A, Kampf C, Sjöstedt E, Asplund A, Olsson I, Edlund K, Lundberg E,

Navani S, Szigyarto CA, Odeberg J, Djureinovic D, Takanen JO, Hober S, Alm T, Edqvist PH, Berling H, Tegel H, Mulder J, Rockberg J, Nilsson P, Schwenk JM, Hamsten M, von Feilitzen K, Forsberg M, Persson L, Johansson F, Zwahlen M, von Heijne G, Nielsen J, Pontén F. (2015) Tissue-based map of the human proteome. Science, 347.

37. Schlam D, Bagshaw RD, Freeman SA, Collins RF, Pawson T, Fairn GD, Grinstein S. (2015) Phosphoinositide 3-kinase enables phagocytosis of large particles by terminating actin assembly through Rac/Cdc42 GTPase-activating proteins. Nature Communications, 6.
38. Lorincz AM, Szarvas G, Smith SME, Ligeti E. (2014) Role of Rac GTPase activating proteins in regulation of NADPH oxidase in human neutrophils. Free Radical Biology and Medicine, 68: 65–71.
39. Lindner SE, Egelston CA, Huard SM, Lee PP, Wang LD. (2020) Arhgap25 Deficiency Leads to Decreased Numbers of Peripheral Blood B Cells and Defective Germinal Center Reactions. Immunohorizons, 4: 274–281.
40. Csépányi-Kömi R, Wisniewski É, Bartos B, Lévai P, Németh T, Balázs B, Kurz ARM, Bierschenk S, Sperandio M, Ligeti E. (2016) Rac GTPase Activating Protein ARHGAP25 Regulates Leukocyte Transendothelial Migration in Mice. Journal of Immunology, 197: 2807–2815.
41. Wang LD, Ficarro SB, Hutchinson JN, Csepanyi-Komi R, Nguyen PT, Wisniewski E, Sullivan J, Hofmann O, Ligeti E, Marto JA, Wagers AJ. (2016) Phosphoproteomic profiling of mouse primary HSPCs reveals new regulators of HSPC mobilization. Blood, 128: 1465–1474.
42. Czárán D, Sasvári P, Horváth AI, Ella K, Sudy AR, Borbély E, Rusznák K, Czéh B, Mócsai A, Helyes Z, Csépányi-Kömi R. (2023) Lacking ARHGAP25 mitigates the symptoms of autoantibody-induced arthritis in mice. Frontiers in Immunology, 14.
43. Czárán D, Sasvári P, Lorincz K, Ella K, Gellén V, Csépányi-Kömi R. (2025) ARHGAP25: a novel player in the Pathomechanism of allergic contact hypersensitivity. Frontiers in Immunology, 16.

44. Jiang YZ, Manduchi E, Stoeckert CJ, Davies PF. (2015) Arterial endothelial methylome: differential DNA methylation in athero-susceptible disturbed flow regions. Bmc Genomics, 16.
45. Vernet R, Matran R, Zerimech F, Madore AM, Lavoie ME, Gagnon PA, Mohamdi H, Margaritte-Jeannin P, Siroux V, Dizier MH, Demenais F, Laprise C, Nadif R, Bouzigon E. (2022) Identification of novel genes influencing eosinophil-specific protein levels in asthma families. Journal of Allergy and Clinical Immunology, 150: 1168–1177.
46. Wisniewski É, Czárán D, Kovács F, Bahurek E, Németh A, Sasvári P, Szanda G, Pettkó-Szandtner A, Klement E, Ligeti E, Csépányi-Kömi R. (2022) A novel BRET-Based GAP assay reveals phosphorylation-dependent regulation of the RAC-specific GTPase activating protein ARHGAP25. Faseb Journal, 36.
47. Chen WX, Lou M, Cheng L, Qian Q, Xu LY, Sun L, Zhu YL, Dai H. (2019) Bioinformatics analysis of potential therapeutic targets among ARHGAP genes in breast cancer. Oncol Lett, 18: 6017–6025.
48. Sebo P. (2024) Chinese authors are overrepresented in medical articles retracted for fake peer review or paper mill. Intern Emerg Med, 19: 2369–2371.
49. (2025) PubPeer. Vol. 2025
50. Cheon H, Xing JC, Moosic KB, Ung J, Chan VW, Chung DS, Toro MF, Elghawy O, Wang JS, Hamele CE, Hardison RC, Olson TL, Tan SF, Feith DJ, Ratan A, Loughran TJr. (2022) Genomic landscape of TCRαβ and TCRγδ T-large granular lymphocyte leukemia. Blood, 139: 3058–3072.
51. Thuault S, Comunale F, Hasna J, Fortier M, Planchon D, Elarouci N, De Reynies A, Bodin S, Blangy A, Gauthier-Rouvière C. (2016) The RhoE/ROCK/ARHGAP25 signaling pathway controls cell invasion by inhibition of Rac activity. Molecular Biology of the Cell, 27: 2653–2661.
52. Barr FG. (2001) Gene fusions involving PAX and FOX family members in alveolar rhabdomyosarcoma. Oncogene, 20: 5736–5746.
53. Han SJ, Jin XY, Hu TY, Chi F. (2023) ARHGAP25 suppresses the development of breast cancer by an ARHGAP25/Wnt/ASCL2 feedback loop. Carcinogenesis, 44: 369–382.

54. Müller C, Oliveira-Ferrer L, Mueller V, Schmalfeldt B, Windhorst S. (2024) Transcriptome-based identification of key actin-binding proteins associated with high metastatic potential in breast cancer. Frontiers in Molecular Biosciences, 11.
55. Zhang Y, Lin Y, Zhu Y, Zhang X, Tao L, Yang M. (2022) ARHGAP25 expression in colorectal cancer as a biomarker associated with favorable prognosis. Mol Clin Oncol, 16: 84.
56. Huang WK, Chen Y, Su HF, Chen TY, Gao JW, Liu YX, Yeh CN, Li SJ. (2021) ARHGAP25 Inhibits Pancreatic Adenocarcinoma Growth by Suppressing Glycolysis via AKT/mTOR Pathway. International Journal of Biological Sciences, 17: 1808–1820.
57. Tzur A, Kafri R, LeBleu VS, Lahav G, Kirschner MW. (2009) Cell growth and size homeostasis in proliferating animal cells. Science, 325: 167–171.
58. Poluri KM, Sarkar S, Gulati K. Protein-protein interactions : principles and techniques. Springer, Gateway East, Singapore, 2021
59. Hayes S, Malacrida B, Kiely M, Kiely PA. (2016) Studying protein-protein interactions: progress, pitfalls and solutions. Biochem Soc Trans, 44: 994–1004.
60. Bruckner A, Polge C, Lentze N, Auerbach D, Schlattner U. (2009) Yeast two-hybrid, a powerful tool for systems biology. Int J Mol Sci, 10: 2763–2788.
61. Paiano A, Margiotta A, De Luca M, Bucci C. (2019) Yeast Two-Hybrid Assay to Identify Interacting Proteins. Curr Protoc Protein Sci, 95: e70.
62. Morris JH, Knudsen GM, Verschueren E, Johnson JR, Cimermancic P, Greninger AL, Pico AR. (2014) Affinity purification-mass spectrometry and network analysis to understand protein-protein interactions. Nat Protoc, 9: 2539–2554.
63. Zhong B, An Y, Gao H, Zhao L, Li X, Liang Z, Zhang Y, Zhao Q, Zhang L. (2023) In vivo cross-linking-based affinity purification and mass spectrometry for targeting intracellular protein-protein interactions. Anal Chim Acta, 1265: 341273.
64. Zhao L, Cong X, Zhai L, Hu H, Xu JY, Zhao W, Zhu M, Tan M, Ye BC. (2020) Comparative evaluation of label-free quantification strategies. J Proteomics, 215: 103669.
65. Roux KJ, Kim DI, Burke B, May DG. (2018) BioID: A Screen for Protein-Protein Interactions. Curr Protoc Protein Sci, 91: 19 23 11–19 23 15.

66. Jorgenson LM, Olson-Wood MG, Rucks EA. (2021) Shifting proteomes: limitations in using the BioID proximity labeling system to study SNARE protein trafficking during infection with intracellular pathogens. Pathog Dis, 79.
67. Zal T. (2008) Visualization of protein interactions in living cells. Adv Exp Med Biol, 640: 183–197.
68. Alam MS. (2022) Proximity Ligation Assay (PLA). Methods Mol Biol, 2422: 191–201.
69. Lin T, Scott BL, Hoppe AD, Chakravarty S. (2018) FRETting about the affinity of bimolecular protein-protein interactions. Protein Sci, 27: 1850–1856.
70. Kobayashi H, Picard LP, Schonegge AM, Bouvier M. (2019) Bioluminescence resonance energy transfer-based imaging of protein-protein interactions in living cells. Nat Protoc, 14: 1084–1107.
71. Murakami Y, Tripathi LP, Prathipati P, Mizuguchi K. (2017) Network analysis and in silico prediction of protein-protein interactions with applications in drug discovery. Curr Opin Struct Biol, 44: 134–142.
72. Jumper J, Evans R, Pritzel A, Green T, Figurnov M, Ronneberger O, Tunyasuvunakool K, Bates R, Zidek A, Potapenko A, Bridgland A, Meyer C, Kohl SAA, Ballard AJ, Cowie A, Romera-Paredes B, Nikolov S, Jain R, Adler J, Back T, Petersen S, Reiman D, Clancy E, Zielinski M, Steinegger M, Pacholska M, Berghammer T, Bodenstein S, Silver D, Vinyals O, Senior AW, Kavukcuoglu K, Kohli P, Hassabis D. (2021) Highly accurate protein structure prediction with AlphaFold. Nature, 596: 583–589.
73. Abramson J, Adler J, Dunger J, Evans R, Green T, Pritzel A, Ronneberger O, Willmore L, Ballard AJ, Bambrick J, Bodenstein SW, Evans DA, Hung CC, O'Neill M, Reiman D, Tunyasuvunakool K, Wu Z, Zemgulyte A, Arvaniti E, Beattie C, Bertolli O, Bridgland A, Cherepanov A, Congreve M, Cowen-Rivers AI, Cowie A, Figurnov M, Fuchs FB, Gladman H, Jain R, Khan YA, Low CMR, Perlin K, Potapenko A, Savy P, Singh S, Stecula A, Thillaisundaram A, Tong C, Yakneen S, Zhong ED, Zielinski M, Zidek A, Bapst V, Kohli P, Jaderberg M, Hassabis D, Jumper JM. (2024) Accurate structure prediction of biomolecular interactions with AlphaFold 3. Nature, 630: 493–500.

74. Lannelongue L, Inouye M. (2024) Pitfalls of machine learning models for protein-protein interaction networks. Bioinformatics, 40.
75. Adhikari H, Counter CM. (2021) Using BioID to Characterize the RAS Interactome. Methods Mol Biol, 2262: 271–280.
76. Bagci H, Sriskandarajah N, Robert A, Boulais J, Elkholi IE, Tran V, Lin ZY, Thibault MP, Dubé N, Faubert D, Hipfner DR, Gingras AC, Côté JF. (2020) Mapping the proximity interaction network of the Rho-family GTPases reveals signalling pathways and regulatory mechanisms (vol 42, pg 128, 2019). Nature Cell Biology, 22: 353–353.
77. Li Y, Wang Y, Zou L, Tang X, Yang Y, Ma L, Jia Q, Ni Q, Liu S, Tang L, Lin R, Wong E, Sun W, Wang L, Wei Q, Ran H, Zhang L, Lian H, Huang W, Wu Y, Li QJ, Wan Y. (2016) Analysis of the Rab GTPase Interactome in Dendritic Cells Reveals Anti-microbial Functions of the Rab32 Complex in Bacterial Containment. Immunity, 44: 422–437.
78. Müller PM, Rademacher J, Bagshaw RD, Wortmann C, Barth C, van Unen J, Alp KM, Giudice G, Eccles RL, Heinrich LE, Pascual-Vargas P, Sanchez-Castro M, Brandenburg L, Mbamalu G, Tucholska M, Spatt L, Czajkowski MT, Welke RW, Zhang SQ, Nguyen V, Rrustemi T, Trnka P, Freitag K, Larsen B, Popp O, Mertins P, Gingras AC, Roth FP, Colwill K, Bakal C, Pertz O, Pawson T, Petsalaki E, Rocks O. (2020) Systems analysis of RhoGEF and RhoGAP regulatory proteins reveals spatially organized RAC1 signalling from integrin adhesions. Nature Cell Biology, 22.
79. Quirion L, Robert A, Boulais J, Huang S, Bernal Astrain G, Strakhova R, Jo CH, Kherdjemil Y, Faubert D, Thibault MP, Kmita M, Baskin JM, Gingras AC, Smith MJ, Cote JF. (2024) Mapping the global interactome of the ARF family reveals spatial organization in cellular signaling pathways. J Cell Sci, 137.
80. BioGRID: Database of Protein, Genetic and Chemical Interactions.
81. Huttlin EL, Bruckner RJ, Navarrete-Perea J, Cannon JR, Baltier K, Gebreab F, Gygi MP, Thornock A, Zarraga G, Tam S, Szpyt J, Gassaway BM, Panov A, Parzen H, Fu SP, Golbazi A, Maenpaa E, Stricker K, Thakurta SG, Zhang T, Rad R, Pan J, Nusinow DP, Paulo JA, Schweppe DK, Vaites LP, Harper JW, Gygi SP.

(2021) Dual proteome-scale networks reveal cell-specific remodeling of the human interactome. Cell, 184: 3022–+.

82. Huttlin EL, Bruckner RJ, Paulo JA, Cannon JR, Ting L, Baltier K, Colby G, Gebreab F, Gygi MP, Parzen H, Szpyt J, Tam S, Zarraga G, Pontano-Vaites L, Swarup S, White AE, Schweppe DK, Rad R, Erickson BK, Obar RA, Guruharsha KG, Li K, Rtavanis-Tsakonas SA, Gygi SP, Harper JW. (2017) Architecture of the human interactome defines protein communities and disease networks. Nature, 545: 505–+.

83. Huttlin EL, Ting L, Bruckner RJ, Gebreab F, Gygi MP, Szpyt J, Tam S, Zarraga G, Colby G, Baltier K, Dong R, Guarani V, Vaites LP, Ordureau A, Rad R, Erickson BK, Wühr M, Chick J, Zhai B, Kolippakkam D, Mintseris J, Obar RA, Harris T, Artavanis-Tsakonas S, Sowa ME, De Camilli P, Paulo JA, Harper JW, Gygi SP. (2015) The BioPlex Network: A Systematic Exploration of the Human Interactome. Cell, 162: 425–440.

84. Hjorth R, Jonsson AK, Vretblad P. (1981) A rapid method for purification of human granulocytes using percoll. A comparison with dextran sedimentation. J Immunol Methods, 43: 95–101.

85. Fischer R, Kessler BM. (2015) Gel-aided sample preparation (GASP)--a simplified method for gel-assisted proteomic sample generation from protein extracts and intact cells. Proteomics, 15: 1224–1229.

86. Sasvári P, Pettkó-Szandtner A, Wisniewski E, Csépányi-Kömi R. (2024) Neutrophil-specific interactome of ARHGAP25 reveals novel partners and regulatory insights. Scientific Reports, 14.

87. Hsiao Y, Zhang H, Li GX, Deng Y, Yu F, Valipour Kahrood H, Steele JR, Schittenhelm RB, Nesvizhskii AI. (2024) Analysis and Visualization of Quantitative Proteomics Data Using FragPipe-Analyst. J Proteome Res, 23: 4303–4315.

88. Ge SX, Jung D, Yao R. (2020) ShinyGO: a graphical gene-set enrichment tool for animals and plants. Bioinformatics, 36: 2628–2629.

89. Hoogendijk AJ, Pourfarzad F, Aarts CEM, Tool ATJ, Hiemstra IH, Grassi L, Frontini M, Meijer AB, van den Biggelaar M, Kuijpers TW. (2019) Dynamic Transcriptome-Proteome Correlation Networks Reveal Human Myeloid

Differentiation and Neutrophil-Specific Programming. Cell Rep, 29: 2505–2519 e2504.

90. Szklarczyk D, Kirsch R, Koutrouli M, Nastou K, Mehryary F, Hachilif R, Gable AL, Fang T, Doncheva NT, Pyysalo S, Bork P, Jensen LJ, von Mering C. (2023) The STRING database in 2023: protein-protein association networks and functional enrichment analyses for any sequenced genome of interest. Nucleic Acids Res, 51: D638–D646.

91. Jumper J, Evans R, Pritzel A, Green T, Figurnov M, Ronneberger O, Tunyasuvunakool K, Bates R, Zidek A, Potapenko A, Bridgland A, Meyer C, Kohl SAA, Ballard AJ, Cowie A, Romera-Paredes B, Nikolov S, Jain R, Adler J, Back T, Petersen S, Reiman D, Clancy E, Zielinski M, Steinegger M, Pacholska M, Berghammer T, Silver D, Vinyals O, Senior AW, Kavukcuoglu K, Kohli P, Hassabis D. (2021) Applying and improving AlphaFold at CASP14. Proteins, 89: 1711–1721.

92. Madeira F, Tinti M, Murugesan G, Berrett E, Stafford M, Toth R, Cole C, MacKintosh C, Barton GJ. (2015) 14-3-3-Pred: improved methods to predict 14-3-3-binding phosphopeptides. Bioinformatics, 31: 2276–2283.

93. Spoerner M, Nuehs A, Herrmann C, Steiner G, Kalbitzer HR. (2007) Slow conformational dynamics of the guanine nucleotide-binding protein Ras complexed with the GTP analogue GTPgammaS. FEBS J, 274: 1419–1433.

94. Svoboda M, Furnelle J, Eckstein F, Christophe J. (1980) Guanosine 5'-O-(2-thiodiphosphate) as a competitive inhibitor of GTP in hormone or cholera toxin-stimulated pancreatic adenylate cyclase. FEBS Lett, 109: 275–279.

95. O'Reilly FJ, Graziadei A, Forbrig C, Bremenkamp R, Charles K, Lenz S, Elfmann C, Fischer L, Stulke J, Rappsilber J. (2023) Protein complexes in cells by AI-assisted structural proteomics. Mol Syst Biol, 19: e11544.

96. Quinn MT. (1995) Low-Molecular-Weight Gtp-Binding Proteins and Leukocyte Signal-Transduction. Journal of Leukocyte Biology, 58: 263–276.

97. Baker MJ, Pan DX, Welch HCE. (2016) Small GTPases and their guanine-nucleotide exchange factors and GTPase-activating proteins in neutrophil recruitment. Current Opinion in Hematology, 23: 44–54.

98. Kouchi Z, Kojima M. (2023) A Structural Network Analysis of Neuronal ArhGAP21/23 Interactors by Computational Modeling. Acs Omega, 8: 19249–19264.
99. Cougoule C, Hoshino S, Dart A, Lim J, Caron E. (2006) Dissociation of recruitment and activation of the small G-protein Rac during Fcgamma receptor-mediated phagocytosis. J Biol Chem, 281: 8756–8764.
100. Fu H, Subramanian RR, Masters SC. (2000) 14-3-3 proteins: structure, function, and regulation. Annu Rev Pharmacol Toxicol, 40: 617–647.
101. Sluchanko NN. (2022) Recent advances in structural studies of 14-3-3 protein complexes. Adv Protein Chem Struct Biol, 130: 289–324.
102. Saha M, Carriere A, Cheerathodi M, Zhang X, Lavoie G, Rush J, Roux PP, Ballif BA. (2012) RSK phosphorylates SOS1 creating 14-3-3-docking sites and negatively regulating MAPK activation. Biochem J, 447: 159–166.

9. Bibliography of the candidate's publications

9.1. Publications relevant to the dissertation

***Sasvári P**, Pettkó-Szandtner A, Wisniewski É, Csépányi-Kömi R.*

Neutrophil-specific interactome of ARHGAP25 reveals novel partners and regulatory insights.

Sci Rep. 2024 Aug 29;14(1):20106. ***doi:*** *10.1038/s41598-024-71002-4*

IF: 3.9

Wisniewski É, Czárán D, Kovács F, Bahurek E, Németh A, ***Sasvári P**, Szanda G, Pettkó-Szandtner A, Klement E, Ligeti E, Csépányi-Kömi R.*

A novel BRET-Based GAP assay reveals phosphorylation-dependent regulation of the RAC-specific GTPase activating protein ARHGAP25.

FASEB J. 2022 Nov;36(11):e22584. ***doi:*** *10.1096/fj.202200689R.*

IF: 4.8

Cumulative impact factor: 8.7

9.2. Publications unrelated to the dissertation

Czárán D, ***Sasvári P**, Lőrincz K, Ella K, Gellén V, Csépányi-Kömi R.*

ARHGAP25: a novel player in the Pathomechanism of allergic contact hypersensitivity.

Front Immunol. 2025 Feb 26;16:1509713. ***doi:*** *10.3389/fimmu.2025.1509713.*

IF: 5.9

Szederkényi G, Kocsis D, Vághy MA, Czárán D, ***Sasvári P**, Lengyel M, Naszlady MB, Kreis F, Antal I, Csépányi-Kömi R, Erdő F.*

Mathematical modeling of transdermal delivery of topical drug formulations in a dynamic microfluidic diffusion chamber in health and disease.

PLoS One. 2024 Apr 11;19(4):e0299501. ***doi:*** *10.1371/journal.pone.0299501.*

IF: 2.6

Bencsics M, Bányai B, Ke H, Csépányi-Kömi R, ***Sasvári P**, Dantzer F, Hanini N, Benkő R, Horváth EM.*

PARP2 downregulation in T cells ameliorates lipopolysaccharide-induced inflammation of the large intestine.
Front Immunol. 2023 Jun 30;14:1135410. ***doi:*** *10.3389/fimmu.2023.1135410.*
IF: 5.7

Czárán D, ***Sasvári P****, Horváth ÁI, Ella K, Sűdy ÁR, Borbély É, Rusznák K, Czéh B, Mócsai A, Helyes Z, Csépányi-Kömi R.*
Lacking ARHGAP25 mitigates the symptoms of autoantibody-induced arthritis in mice.
Front Immunol. 2023 May 10;14:1182278. ***doi:*** *10.3389/fimmu.2023.1182278.*
IF: 5.7

Cumulative impact factor of all publications: 28.6

Cumulative impact factor of first author and shared first author publications: 3.8

10. Acknowledgements

First and foremost, I would like to express my sincere gratitude to my supervisor, **Dr. Roland Csépányi-Kömi**, for his continuous support and insightful feedback throughout the course of my research and the thesis writing.

I am also deeply thankful to the **present and former members of our research laboratory** for creating a welcoming, supportive, and intellectually engaging atmosphere. In particular, I would like to specifically thank **Prof. Dr. Erzsébet Ligeti** for the foundations she laid for our research projects, **Regina Tóth-Kun** for her remarkable technical aid and endless eagerness to help, as well as **Dr. Éva Wisniewski** and **Domonkos Czárán** for their extensive and meticulous work that led to the creation of several manuscripts.

My gratitude extends to the former and current heads of the department—**Prof. Dr. László Hunyady** and **Prof. Dr. Attila Mócsai**—for providing a supportive academic environment and for facilitating the resources necessary for accomplishing this research.

I am incredibly grateful to my **family and friends** for their unwavering love, patience, and faith in me throughout this journey. Thank you for your encouragement and for maintaining balance and happiness along the way.

Finally, I wish to express my heartfelt gratitude to my **fiancé** for his unending support, understanding, and kindness during both the most challenging and the most rewarding moments of this experience. Your presence has been a constant source of strength and joy.